M. Tech (Computational Design)

[Sudhanshu Sharma]

2019

ANALYSIS OF CONTACT STRESSES FOR RAIL-WHEEL INTERFACE

A PROJECT REPORT

SUBMITTED IN PARTIAL FULFILLMENT OF THE REQUIREMENTS

FOR THE AWARD OF THE DEGREE

OF

MASTER OF TECHNOLOGY

IN

COMPUTATIONAL DESIGN

Submitted by:

SUDHANSHU SHARMA

(2K17/CDN/05)

Under the supervision of

Prof. A K AGRAWAL

DEPARTMENT OF MECHANICAL ENGINEERING

DELHI TECHNOLOGICAL UNIVERSITY

(Formerly Delhi College of Engineering)

Bawana Road, Delhi-110042

JUNE, 2019

DEPARTMENT OF MECHANICAL ENGINEERING,

DELHI TECHNOLOGICAL UNIVERSITY

(Formerly Delhi College of Engineering)

Bawana Road, New Delhi -110042

CANDIDATE'S DECLARATION

I, Sudhanshu Sharma, Roll No. - 2K17/CDN/05 student of M.Tech (Computational Design), hereby declare that the project dissertation titled 'Analysis of contact stresses for rail-wheel interface' which is submitted by us to the Department of Mechanical Engineering, Delhi Technological University, Delhi in partial fulfillment of the requirement for the award of the degree of Master of Technology, is original and not copied from any source without proper citation. This work has not previously formed the basis for the award of any degree, diploma associateship, fellowship or other similar title or recognition.

Place: New Delhi **Sudhanshu Sharma**

Date: (**2K17/CDN/05)**

DEPARTMENT OF MECHANICAL ENGINEERING,

DELHI TECHNOLOGICAL UNIVERSITY

(Formerly Delhi College of Engineering)

Bawana Road, New Delhi -110042

CERTIFICATE

I hereby certify that the Project Dissertation titled "Analysis of contact stresses for rail-wheel interface" which was submitted by Sudhanshu Sharma, Roll No. - 2K17/CDN/05 Department of Mechanical Engineering, Delhi Technological University, New Delhi in partial fulfillment of the requirement for the award of the degree of Master of Technology, is a record of the project carried out by the student under my supervision. To the best of my knowledge this work has not been submitted in part or full for any Degree or Diploma in this University or elsewhere.

Place: Delhi

Date:

Prof. A K AGRAWAL

SUPERVISOR

Professor

Department of Mechanical Engineering

Delhi Technological University

ABSTRACT

The central idea of all the research of locomotive and track interaction is dependent on Wheel and Rail contact. The contact zone produced by interaction of rail and the wheel is the reason for all the power and load transmission. The contact patch developed is also subjected to high stress intensity and hence prone to failure. Therefore there is a need to study this contact patch, so as to have better knowledge of rail-wheel dynamics.

Finite Element Analysis Software package presents a fairly reliable way to model and evaluated the real life conditions of the contact problems. But meticulous study of contact is very time consuming task and often requires high performance computing. With suitable assumptions, a tradeoff between computing time and accuracy can be achieved. Conventionally, Hertz contact model is used to calculate contact pressure analytically. Though, some of Author's assumptions are breached in actual practice. Nevertheless, his formula is relatively easier to verify the results based on the major and minor axes of the ellipse.

In the current thesis, with the supplement of literature review, various contact parameters (including contact pressure, frictional stress and penetration) and structural results are produced by usage of FEA solver. Later comparison of the work has been done analytically using the Hertzian contact model. With preserving good computational effectiveness and fair amount of accuracy all the above said parameters were studied. The expertise achieved from this work illuminates the future research direction in the arena to contact of rail-wheel interface.

ACKNOLEDGEMENT

The efficient and effective completion of the project is unfinished without giving the acknowledgement to everyone who made it feasible and the person whose guidance and support was very crucial.

I owe a lot to my supervisor, Prof. Atul Kumar Agrawal, Professor, Department of Mechanical Engineering, for supporting and guiding to explore the depth in the search of knowledge and creativity. I would like to thank him for all the assistance and being a source of motivation whenever needed.

I am obliged to everyone who directly or indirectly lent his/her support for successful completion the task. I would like to thank the Department of Mechanical Engineering for providing us advanced computational lab facilities for producing efficient work.

In the end, I thank my parents for always being supportive.

Contents

1. Introduction 1
   1.1 Indian Railways 1
   1.2 Railway mishaps and their causes 2
   1.3 Failures attributed to contact wear 5
2. Literature Review
   2.1 Studies on contact stress 9
   2.2 Motivation 18
   2.3 Research Gap 18
3. Proposed Methodology 19
   3.1 Hertzian Contact Model 19
   3.2 Nature and Region of contact 22
   3.3 Solving Contact Problem by FEM 24
      3.3.1 Different types of contact 26
      3.3.2 Contact and target surface designation 27
      3.3.3 Asymmetric Contact and Symmetric Contact 27
      3.3.4 Direct Solver vs. Iterative Solver 28
   3.4 Development of CAD model 29
   3.5 Ansys Workbench 18.2 30
      3.5.1 Material Properties 30
      3.5.2 Model 31
      3.5.3 Material Assignment 31
      3.5.4 Contact Initialization in the FEA Solver 32
      3.5.5 Contact Between rail and the wheel 33
      3.5.6 Contact between Axle and the wheel 33
      3.5.7 Boundary Condition Definition 34
      3.5.8 Discretization of model 36

3.5.9 Analysis Settings 38
3.5.10 Setting up loads 38
3.6 Archard Wear 40
3.7 Modeling wear at contact interface 43
3.8 Verification of model using Hertzian Method 44
3.9 Verification of contact pressure using Hertzian Method 45
4. Benchmarking Problem of cylinder on plate 46
4.1 Problem Description 46
4.2 Boundary Condition 46
4.3 Contact Condition 47
4.4 Mesh Element 48
4.5 Results 48
4.6 Mesh Convergence 51
4.7 Verification of model using Hertzian Model 52
4.8 Verification Of Contact Pressure using Hertzian Method 53
4.9 Percentage Error in Solution 54
5. Results 55
5.1 Analytical Results 55
5.2 Computational Results 55
5.2.1 Equivalent Von Mises Stress 55
5.2.2 Contact Pressure 56
5.2.3 Contact Patch Size 58
5.2.4 Contact Status 60
5.2.5 Penetration at contact region 61
5.3 Comparison of analytical and computational results 62
6. Conclusion 64
References 65

List of Tables

Table no.	Table name	Page no.
1.1	Statistics of accidents and corresponding causalities	3
3.1	Application of displacement to the axle w.r.t. time	39
4.1	Contact Forces variation with time	49
4.2	Mesh Convergence	51
4.3	Comparison of Benchmark problem Results with Hertz contact theory	54
5.1	Comparison of FEM and Hertz Contact Stress	62
5.2	Comparison of FEM and Hertz Contact Patch Size	63

List of Figures

Figure no.	Figure name	Page no.
1.1	Derailment took place Raja-Rani Express in 2017	2
1.2	Break-up of number of Accidents by Accident category	4
1.3	Break-up of number of Causalities by Accident category	4
1.4	Plastic flow of metal from top surface to side face	6
1.5	Effect of contact stress leading to plastic failure in wheel (Above) and crack growth in rail due to rolling contact Fatigue (Below)	7
1.6	Chipping of material from the side and top surfaces respectively	7
3.1	Shape of contact patch and pressure distribution	20
3.2	Hertzian coefficients	21
3.3	Functional zones in rail wheel contact	22
3.4	Interacting master and slave at the interface	25
3.5	Schematic picture of pure penalty algorithm	26
3.6	Schematic diagram of rail and wheel profiles	29
3.7	Ansys Workbench with static Structural module	30
3.8	Description of Engineering data and material properties	31
3.9	Material assignment to CAD geometry	32
3.10	Wheel is defined as contact body and rail as target body in rail wheel interface	33
3.11	Axle surface is defined as contact body and wheel bearing zone as target body at wheel axle interface	34
3.12	Fixed boundary condition in rail	35
3.13	Axle surface was given freedom to move in x- direction w.r.t. ground	35

3.14	Wheel was allowed to move in x and y direction and freedom to rotate with z as reference.	36
3.15	Face selection in progress for reefing the mesh size	37
3.16	Discretized model with very fine mesh at interacting surface of rail and wheel	37
3.17	Selection of analysis Settings in ‘Detail’ box	38
3.18	Bearing load application in downward direction	39
3.19	Joint load application in positive x- direction	40
3.20	Wear Sub-Routine initialization in Ansys APDL	43
4.1	The diametric cut is displaced vertically down by 10.16 mm	46
4.2	Firs Ramp load of 312057 N is applied	47
4.3	Assigning of master and slave contact condition	47
4.4	Plot of contact forces due to contact stress in y-direction	48
4.5	Comparison of Von Mises Stresses of Different Mesh Size	49
4.6	Equivalent Deformation	50
4.7	Comparison of contact pressure for penalty (left) and kinematic algorithm (right)	50
4.8	Variation of contact Pressure w.r.t. no. of nodes	51
5.1	Variation of Equivalent Von Mises stress w.r.t. time	56
5.2	Contact patch formation at the interface (without wear)	56
5.3	variation of contact Pressure w.r.t. time (without wear)	57
5.4	Contact patch formation at the interface (with wear)	57
5.5	Semi major axis ‘a’ (without wear)	58
5.6	Semi minor axis ‘b’ (without wear)	59
5.7	Semi major axis ‘a’ (wear)	59
5.8	Semi minor axis ‘b’ (wear)	60
5.9	Contact Status between rail and wheel interface	60
5.10	Contact Status between rail and wheel	61
5.11	Penetration occurring at rail and the wheel interface	61
5.12	Variation of penetration at contact region w.r.t. to time	62

List of Symbols

Symbol	Interpretation
P_0	Maximum Contact pressure
b	Semi minor axis
a	Semi major axis
F	Load (Vertical)
m, n	Hertzian Coefficients
θ	Theta (Angle)
R	Radius
m	Metre
N	Newton
MPa	Mega Pascal
s	Second
mm	Milli Metre
KN	Kilo Newton
μ	Poisson's Ratio
f	Friction coefficient
u	Deflection
K	Stiffness
E	Young's Modulus of Elasticity

x,y	coordinate axes
τ	Shear Stress
γ	Shear Strain

CHAPTER 1 : INTRODUCTION

Railway is one of the most cost efficient modes of transportation for carrying passengers or shipment between two sites via land. Recently there was a hike in railway problems. Therefore there is a need to study the rail wheel contact parameters. We are heading to a technological age where we have more axle load, close turning curves, lighter weight vehicle and increased velocities. Yet, these varied necessities are all depending upon same targets i.e. increased reliability, reduced maintenance cost and more safety.

To tackle such a complicated requirement, an amalgamation of knowledge of different disciplines like mathematics, mechanical and physical sciences are required. This project tries to study the rail wheel interface parameters on basis of gathered information of many railway researchers, scientists and explorers of the railway arena.

The general idea of this chapter is to encourage study of contact patch in rail wheel dynamics which is the key concept around which rail wheel parameter are dependent.

1.1 Indian Railways

Ministry of Railways manages and operates India's railway system called Indian Railways. Indian Railways has 121,407 km of track over a route of 69,182 km making it 4^{th} largest network. The average speed of freight is around 24 km/h [2]. Averages of 20,000 passenger trains run daily on sub urban and long distance routes [1]. Express trains have an average speed of 50.6 km/h. Electrification of routes (49 %) with 25 kV AC is done. Indian Railways employs 1,308,000 (March 2017) employees making it 8^{th} largest employer in the world. Indian Railways transported 1.16 billion tons of freight and moved 8.26 billion commuters in the year terminating in March 2018. Also Indian Railway had revenue of almost 27 billion USD in the year 2017-18. Therefore there is very high dependency on Railways in the economy of the country.

A relative study of Worldwide Railways demonstrate that India ranks 1^{st}, as far as number of passengers travelling per km is concerned but lacks considerably in the field

of latest technology used by other countries [18]. The vision of Ministry of Railways for coming years is oriented towards high speed railways, improved safety and world class facilities.

However, we are still lacking the infrastructure for adoption of new technology.

1.4 Railway mishaps and their causes

Railway Mishaps are majorly classified into following classifications:

1. Derailments
2. LCs (Level Crossings)
    a. Manned LCs
    b. Un-manned LCs
3. Accidents due to fire hazard
4. Collisions
5. Miscellaneous – For Example Natural Disasters (landslides, earthquake, floods etc.)

Fig.1.1: Derailment took place Raja-Rani Express in 2017

Table 1.1: Statistics of accidents and corresponding causalities

S. No.	Description	2012-13	2013-14	2014-15	2015-16	2016-17	Total
1	Cumulative Number of Accidents	122	118	135	107	104	**586**
2	Break-up of Accidents by category						
	Derailments	49	53	63	65	78	**308**
	Manned LC	5	4	6	6	0	**21**
	Un-manned LC	53	47	50	29	20	**199**
	Collisions	6	4	5	3	5	**23**
	Fire hazard	9	7	6	0	1	**23**
	Miscellaneous	0	3	5	4	0	**12**
3	Total number of casualties by Accident category	204	152	292	122	241	**1011**
	Derailments	5	6	104	36	196	**347**
	Manned LC	18	6	31	12	0	**67**
	Un-manned LC	123	98	130	58	40	**449**
	Collisions	27	1	15	1	5	**49**
	Fire hazard	31	35	0	0	0	**66**
	Miscellaneous	0	6	12	15	0	**33**

An Investigation of above statistics aggregated over the phase of 2012-13 to 2016-17, project the succeeding vital insights [19]:

1. Derailments are the causes for more than 50 percent of the total accidents however LC related accidents (Manned + Unmanned) accounted for 40 percent.
2. 35 percent of the total causalities were a consequence of derailments.
3. At last, derailment and LC accounted for total 82 percent injured people together.

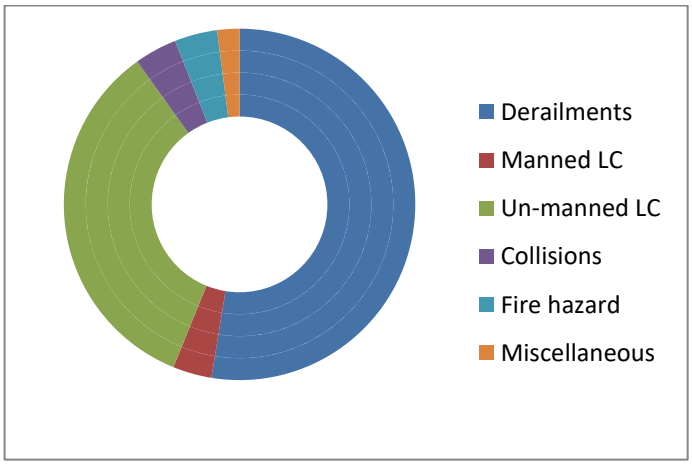

Fig.1.2: Break-up of number of Accidents by Accident category

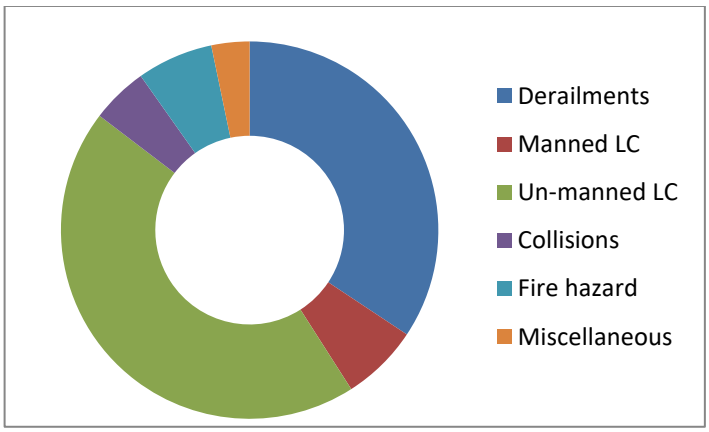

Fig.1.3: Break-up of number of Causalities by Accident category

The statement of Safety Review Committee presented in 2012 submits, following causes behind such failures:

1. Derailment – They are primarily caused by fractures in rails caused during manufacturing, installation, extreme weather conditions etc.
2. Negligence – 60 percent of mishaps occurred due to carelessness of railway staff according to NITI Aayog.
3. Improper Design – In 2015, almost 859 railway accidents occurred due to defected and faulty track according to NCRB (National Crime Records Bureau).
4. Less Investment in Safety
5. Increased Traffic – The statement by committee stated railway routes have increased by only 23 percent since 1950 to 2016 and passenger and freight traffic has increased from 1344 percent to 1642 percent.

1.3. Failures attributed to contact wear

Continuous interaction of rail wheel interface results in high frictional stress, contact pressure and ultimately wear. Wear could be established as the indirect cause of derailment. Therefore there is a need to look into mechanism of wear at rail wheel interface. Derailments generally are caused because of Rolling Contact Fatigue.

Wear does not directly cause the derailments, but act as a primary sponsor in many ways. Wear modifies wheel and rail profile, which as a matter of fact changes the nature of contact between rail and wheel and consequently may increase the Rolling Contact Fatigue rate, and results in shallow crack propagation in rails.

Rolling Contact Fatigue can trigger damage and can lead to surface crack by the action of wear on the rail or by plastic deformation of the material. A first, Rolling Contact Fatigue initiates tiny cracks which grow at shallow angle, and sometimes turn towards steep angle. Wheel-Rail wear can be predicted by simulation models in a very cost efficient way. The other benefit is that wear and rolling contact fatigue can be known beforehand. Archard's wear model is has proved to produce good results.

Wear plays an important role in derailment (degradation) of rail-wheel and it is directly related to reduce the life of rail, limiting the performance of rail and considerably increasing the life cycle cost of the rail tracks.

Rail generally suffers from very high stresses and has complicated stress zone with bending stresses, contact stresses and thermal stresses acting at a time. According to the perspective of a maintenance engineer, contact stress management should be done meticulously because RCF and plastic wear are directly affected by contact stresses.

The most common type of wear occurs when metal is removal takes place between the rail and the wheel due to abrasion. Parameters like load, nature of contact, complicated stress fields, etc. have direct impact on the wear mechanism. The primary mechanisms of wear at the rail wheel interaction are abrasion, oxidation, fatigue related and adhesion. Additionally, wear in rail generally occurs at top surface (head wear), or on side surface (known as gauge face wear) or at the combination both top and side faces. Area prone to wear is manifested by loss in material or plastic flow of metal. Thus, the profile of rail gradually changes because of high train traffic, enormous contact stresses, environmental conditions, etc. leading to failure.

Fig.1.4: Plastic flow of metal from top surface to side face

Fig.1.5: Effect of contact stress leading to plastic failure in wheel (Above) and crack growth in rail due to rolling contact Fatigue (Below)

Fig.1.6: Chipping of material from the side and top surfaces respectively

The contact stresses in case of rail and wheel interaction leads to wearing of both the surfaces which are in contact. At first, wear was considered the only reason of failure at the rail wheel interface. Although, with the improvement of running gear, better tolerances of rail and wheel profile, better material selection, proper lubrication etc. wear became less significant.

There are many types of wear in rail and wheel, although adhesion wear and delamination wear are primary ones to understand wear mechanisms. In case of adhesion, due to large number of cycles tiny flakes are generated at the contact region. After sometime, these flakes break away, leaving shiny metal surface. Adhesion is mild wear. Delamination wear is more dangerous form of wear. In case of delamination crack initiation takes place on the surface and then crack propagates into the surface. Sometimes that crack returns to the surface after taking a turn, hence a flake is removed. This new generated surface is more irregular than the surface produced during adhesion wear. Rolling contact fatigue crack initiation can take place both on sub surface (10-25 mm) or on periphery, although deeper cracks are the result of the material defects. In both Rolling Contact Fatigue and Delamination there is similar way of crack initiation i.e. by repeated contact among the surfaces, plastic limit is reached and initiation of crack takes place. Rolling Contact Fatigue takes place when contact conditions are more severe than that of delamination. The crack propagates in such a way that it reaches other surface crack and removes a chunk of material from the surface.

CHAPTER 2: LITERATURE REVIEW

Literature survey is done in two sub sections, which are detailed below.

2.1 Studies on contact stresses

Dukkipati et al. [3] gave the formulation of creepage with the incorporation of lateral radius of rail and other kinematic parameters. Creep forces were evaluated according to Kalker's linear theory; hence author made an assumption –ellipse shaped contact patch with minute creepage and substantial friction coefficient, hence effective slip becomes minimal for the entire contact area. Kalker improvised his linear theory in FASTSIM and suggested a displacement constitutive principle which constituted material derivatives of relative displacements in case of interacting rail/wheel profile, that are known as compliant parameters L_x and L_y (longitudinal and lateral). Author has also described about the Hertzian parameters "n" and "m" in his book, calculated by regression method.

Ramanan et al. [4] concentrated on the issue of evaluating the contact stresses by the implementation of elasto-plastic methodology at local and global locations. Author has focused on stress analysis from the coupled effect of both mechanical and thermo mechanical on a three dimensional contact model. He demonstrated that the wheel is having a lateral movement while moving freely on the rail. Therefore FEA solver should be allowed to have degree of freedom in side way direction, while defining the boundary condition. Author laid emphasis on the fact that as the region of contact indicate yield point, elastic theory becomes imprecise and instead plastic theory should be taken into consideration for evaluating strength for rail-wheel. He concluded that stresses are more during braking condition than that of steady motion with payload carrying condition.

Yan et al. [5] presented an investigation of applicability of hertz theory in wheel and rail contact problem. A 3D model was developed for analyzing the interaction between rail and the wheel in FEA tool. In addition to standard UIC60 rail, crane rail (Cr135) is also

considered for comparison of FEA results. Simulations were performed on standard UICORE wheel profile for varied transverse locations. As long as plastic deformation does not takes place Hertzian theory shows good agreement with FEM results. Dissipated power is calculated once the model is established and verified with Hertz theory. Power dissipation appears due to differences in regional distortion velocities. A substantial divergence from Hertzian theory occurs when plasticity introduced. Although in this case the average distribution of contact pressure increases but maximum contact stresses are lower than that of elastic case.

Telliskivi et al. [6] presented work in contact mechanics to evaluate rail wheel profile topology using FEM approach. X1 and X10 trains are selected, which are moving in single direction and are taking a sharp turn of radius 303m. Two test cases are contrasted for their results from CONTACT package and Hertz model. In the 1^{st} instance the contact with rail gauge corner is considered with the wheel whereas,, in 2^{nd} condition rail head is considered to have contact with wheel. Evaluation of contact pressure by both CONTACT and Hertz is done. While simulating the results for the 1^{st} case a vast difference in the results of CONTACT, Hertz model and FEM were observed. Results FEA were one-third of the one produced by CONTACT and Hertz solution. This immense difference is values were attributed to half space assumption of Hertz and also because of the plasticity introduced in the material modeling. In the 2^{nd} instance, the contact pressure by CONTACT, FEM and Hertzian model provides matching results. Data of two years is recorded for commuter train such that track hardness was documented for 2D profile. Experimentation reveals that there was a noteworthy change in profile due to plastic flow in the rail used for 5 years.

CAD Modeling was implemented in design modeler tool of ANSYS. Appropriate material properties (plasticity, hardening factor, yielding standards, etc.) were chosen from the material library of ANSYS workbench. Stress strain curve as specified by manufacturers of rail and wheel were taken as input for imparting kinematic hardening to the FE model. Identification of forces acting on the model while train maneuvers curve is anticipated by multi body dynamics packages like MEDYNA. A total of 5000 elements (rail and wheel) and 3000 at contact were created, before furnishing model for analysis. Author concluded that maximum stresses (von Mises) were 606 Mpa for a

model which incorporated plasticity. When rail head is in contact with the wheel then, the results of CONTACT, FEM and the Hertzian model offers a great agreement to one another. This happen because of the half space assumption i.e. the contact patch size is very small w.r.t. dimension of the contacting bodies.

Jiang et al. [7] presented study on elastic and plastic 3D model of rail/wheel contact. The paper propositioned model having cyclic plasticity incorporating ratcheting behavior. Author performed his analysis on Abaqus package. *Sebes et al*. amended the model (STRIPES) propositioned by *Ayasse,* for ideally elastic characteristic by employing semi and multi Hertzian techniques. *Sebes et al.* recommends assuming the contact to be elastic produces impractical results; hence there is a need to look into plastic behavior for determining fatigue characteristics of rail/wheel model. Author found out that stresses (contact) were coherent with plastic behavior; suppositions are made to incorporate plasticity into the contact model. Analogous methodology was incorporated by *Sebes* for evaluating Multi-Hertzian contact model, which implemented plasticity. The lone distinction occurred during the selection of ellipse experiencing inter penetration. Contact angle function is the criteria for selecting the ellipse denoted by y.

$$\sum_j N_j cosy_j = Q \qquad (1.2)$$

Where Q = Vertical Load

Fisher et al. [8] presented an approximate solution of the Hertz's contact model. Author gave an alternative to elliptical integral involving into the calculation of rail wheel contact model. Author calculated approximate solution for semi major *(a)* and semi minor axes *(b)* of the contact patch ellipse *(P_0),* maximum pressure of the contact patch, the mutual approach. The analytical method was used to compare the results for four types of rail wheel contact configurations i.e. Wheel/Crossing (new), Wheel/Crossing (worn), Wheel/rail (new) and Wheel/rail (worn). Author concluded that the relations were exact for a spherical contact problem and is also valid for slim contact patches which are produced in case of wheel and the central region of crossing.

Weist et al. [9] compared the methods for calculating contact pressure at wheel-rail contact including the models based on Hertzian theory and Kalker's CONTACT with

Finite Element solutions using Abaqus. Contact pressure results from the half space models were in agreement with finite element model for the case when wheel is assumed elastic in nature. However, when half space models are compared with elasto-plastic FE models, significant discrepancies occurred, implying the importance of using elastic-plastic calculations for study of contact characteristics. Wen et al. investigated the wheel-rail contact under partial slip conditions and varying contact loads and developed a three dimensional finite element model to analyze wheel-rail rolling contact using cyclic plasticity. The contact patch was obtained by Kalker's CONTACT and FE method was modified by inculcating plasticity theory. The author confirmed the presence of a wavy rolling contact surface rail profile due to varying normal contact force.

Wu et al. [10] included the thermal aspects of rail wheel sliding contact into his research and developed a finite element model to study thermo-elastic-plastic deformation and residual stress on rail. The normal contact pressure was idealized Hertzian in nature. Temperature dependent material parameters including thermal coefficient are considered and its effect on residual development and equivalent plastic strain is studied. The research helped in understanding mechanism of rail-wheel frictional thermal fatigue under different service conditions.

Arslan et al. [11] presented the analysis of half three dimensional model of rail wheel contact patch using FEA. Author was motivated to present his work due to the fact that most of the earlier work was done on either two dimensional axisymmetric or very basic three dimensional models with very poor mesh quality or quantity or both. Author developed geometric model then did the finite element analysis in Ansys Software package. Rail being softer material was assigned Young's Modulus of 200 Gpa while that wheel being 210 Gpa. After the application of analysis setting and boundary conditions, bi-linear kinematic hardening elastic plastic material model was imported. Inclusion of the shaft in the wheel, while performing rail/wheel contact analysis, makes the model more realistic. Author notices that because of the wheel is harder than the rail therefore plastic deformation is more prevalent in rail than in wheel. Equivalent Von Mises stresses and strains are found within the limit. Contact patch both at the rail and

the wheel were studied and were in the form of ellipse with maximum pressure at the center of the patch.

Zong et al. [12] presented a study of rail ends under loading due to wheel motion and generated contact. Presented work focuses on the consequence of disjointedness of rail ends and existence of insulation with low modulus at the disparity, with deviation of stresses in IRJ. 3D CAD geometry is facilitated to an FEA solver for analysis. It's revealed from the study that stresses have maximum value at sub-surface of rail head, at the time when contact patch is at a distance away from rail end, and drifts toward rail surface as wheel moves towards the end of the rail. Due this displacement of contact patch enhanced stress concentration levels are endured by insulation and rail ends. Modulus of elasticity of rail end and the modulus of elasticity of insulation has direct impact on stress concentration. Higher is the modulus, lower becomes the stress concentration in end of the rails, although increased stresses in the insulation, hence the failure. High level of discretization on solid element 3D8 was developed in ABAQUS framework. Finer mesh at the interacting surface whereas coarser (3DR8) mesh on the far body was implemented. Assumption is made such that the insulation remained glued to the ends of the rail. Author concluded that model follows Hertzian theory as long as the $l/a > 0.960$. Von Mises stresses and the contact stresses at the interaction of insulation and ends of the rail are very susceptible to contact location of wheel. As wheel approaches rail end, stresses shoots up and rail head dame process picks up the pace. If the modulus of elasticity of the insulation and ends of the rail becomes almost equal, the stresses at rail ends gets subsidized, although there is still higher stresses induced in the insulation, which results in pre mature failure.

Trummer et al. [14][20] categorizes RCF mechanisms to investigate possible causes of impairment on rail and wheel into 4 divisions: 1. T_y Approach, 2. Ratcheting method, 3. Shakedown concept, 4. Fracture Mechanics. In one of his papers, author focused on a ratcheting model employing elastic contact computations. To deal with 3-D obstruction, a new 2.5D approach is suggested which exercises a 2-D model to guesstimate 3-D problem by dividing the rail head into equal fragments of finite breadth. Each fragment

is depended upon the tangential and normal loads acting on its top. These loads are evaluated using elastic constants. Plastic distortion mechanism is also investigated.

Srivastava et al. [15] presented the study of contact stresses by both FEM and Hertzian method for Indian standard rail wheel profile. Author studied the effect of effect of 6 different radii for rail and wheel topology and wheel profile taper on contact parameters of interacting rail wheel profile. Additionally, fatigue life and effect of repeated loading is studied. Timoshenko approach is followed for analytical articulation of the problem. Standard results of contact is presented for 1 mm mesh size, as it is found that discretization density has direct impact on the accuracy of the solution. After finding the stress distribution using Finite Element Analysis, the consequence of crack (which is produced due to fatigue loading) on normal loading are explored. This application is used for finding the life, after the effect of fatigue crack is considered. This study aims to have direct appliance towards design of rail wheel topology. A fairly accurate polynomial Hertzian Contact model is used in place of one with elliptical integral. It is well found out by the author that polynomial estimate has decent association with FEA results. Author has equated the end results of analytical solution (Hertz), FEM and Kalker's method. Author also focuses on evaluation of fatigue life and damage on rail road through analytical solution by applying multiple axes crack (fatigue) model as given:

$$FP = \left(< \sigma^{max} > \frac{\Delta \epsilon}{2} \right) + J \Delta\tau \Delta\gamma \qquad (1.1)$$

Where $<\cdot>$ refers to MacCauley braces, used as $< z > = 0.5(|z| + z)$

$\Delta\tau$ = Shear Stress (normal to crack plane)

$\Delta\gamma$ = Shear Strain (on crack plane)

σ^{max} = Max. Normal Stress

J = Constant (alters with material and load)

Author explains about the problem being a nonlinear application takes a lot of computation time for facilitating results. For that reason, only a sector the wheel is only considered and then imported into the Ansys package. SOLID186 element is used for rail and the wheel bodies and CONTA174 and TARGET170 is correspondingly used for contact and the target surfaces which are wheel and the rail respectively. Total mass is around 80 ton which means effectively 10 ton on each wheel. Assumption is made that wheel moves on straight path. Therefore, a load 98100 Newtons acts on bearing.

Author concludes from the study that there is a decrement stress when with increase in topology radius, as well as increase in breadth and decrease in longitudinal dimension. Hence, more probability of sliding friction happens. Higher taper in wheel leads to diminution in contact area. The results furnished from Finite Element Analysis are keyed into fatigue analysis to evaluate no. of cycles before failure and damage due to fatigue. A precipitous fall in fatigue life is observed when load is more than 100000 N. Fatigue life appears to be impervious towards change in rail wheel profile topology.

Sharma et al. [18][16] presented work on dynamic analysis of rail wheel contact using finite element analysis. Author's exhibits the effect of topology of rail and the wheel in contact analysis. All the analysis was done on standard UIC-60 rail profile and corresponding wheel. Analytical study is presented using Quasi Hertz method followed by finite element analysis to investigate the effect of rail wheel profile on the distribution of contact stresses and size of contact patch. This comprehensive study also includes impact of contact forces and stresses on the wheel which is rolling on the rail surface. Kalker's linear theory was also implemented to investigate the consequence of lateral motion of surfaces in evaluating the frictional stresses. All the analysis was done in elastic region of rail wheel contact. Methodology includes construction of a hypothetical grid around the contact patch for both wheel and rail and then the approximate pressure distribution of the elliptical curve is found analytically. Finite element analysis was done considering hex dominated mesh for variety of configurations like varied conicity, different wheel and rail profiles. Author has validated the fact that as the rail inclination increases, contact pressure also increases. Author concluded from the results that there is a decrease the contact stresses with the increase in rail profile, also increasing the radii of wheel leads to decrease in major axis and increase in minor

axis of the contact patch, thus higher sliding friction. Additionally, stimulus of wheel taper causes enhancement of length and reduction in minor axis of contact patch ellipse, thus decrement in sliding friction. The patch size has a lot of dependency on the rail wheel topology. Author found out from his study that the highest creep force was around when ξy was 0.1.

The conclusion was based on the fact established that rail wheel profile has crucial effect on the pressure distribution. Rail wheel topology gets alter by lateral motion of the wheel over the rail, hence the contact pressure, contact patch parameters and its location.

Pun et al. [17] studied and evaluated the ratcheting performance of different steel grades under different wheel-rail cyclic rolling contact conditions. The paper used a hybrid approach by combining non-Hertzian contact pressure and Carter's theory to simulate wheel-rail rolling contact.

Lorenzo et al. [19][20] studied the influence of conformity on wheel-rail rolling contact mechanics. He suggested that Hertzian assumption of punctual contact between wheel and rail i.e. assumption that the size of the contact patch is much smaller than the corresponding dimensions of the body, implies flatness of the contact area and therefore, does not hold correct for a wheel-rail conformal contact for a curved contact patch. The author studied the effect of conformity on normal and tangential parts of rail-wheel contact and suggested influence factors (direct and cross influence coefficients) to switch elastic puzzle of half spaces to puzzle of conformal contact. Furthermore, author studied 3D contacts with friction by using FE models and an augmentation of exact contact hypothesis referred as CECT (Conformal Exact Contact Theory).

Ciotlaus et al. [23] presented a study of interaction between rail and wheel and its effect on rail and wheel wear. Author investigated the association between rail and rolling wheel wear and dealing strategy for improved rail safety, maintenance planning and noise avoidance. Author takes two sources of stresses in consideration which are residual stresses in manufacturing and stresses induced due to rolling motion of the wheel. Author studies 7 years of statistics of Romanian Railway and establishes a connection between rail wheel defect and how maintenance is the major element in rail crack avoidance. The major defects that occurred in Romanian railways over 7 year

period were Defect type 70.2 (horizontal head tear), Defect type 53.1 (web defect) and Defect type 76.3 (horizontal head split due to poor welding). Author's major finding was that poor manufacturing processes lead to the defected rails, which ultimately lead to accidents. Author found that contact patch which changes its position continuously is one of the key reasons of wear. Appearance of transverse fissure defects shows that poor maintenance and surveillance are equally partners in crime to be blamed.

Fukagai et al. [24] presented a study describing the transitions that occur in rail wheel contact during running in. Author reveals that the traction coefficient has direct impact on the derailments. Higher is the value of traction coefficient more is the probability of wheel climb derailment. There scenario is more prevalent after wheel machining. Author investigates on the consequence of increased traction coefficient on progression of rail wheel contact at the time of running in. Methodology involved experimental work in which a full size test rig model was developed and was mounted with ultrasonic transducers arranged in a sequential manner. Contact stiffness coefficient was evaluated as the result of the experiment. As it turns out stiffness of the interface is directly proportional to traction coefficient. But there is a slight delay in rise of traction coefficient as because of conformal geometry at the contact zone, contact stiffness increases first. Author aims to provide a foundation so that the cases of derailment decline.

Author has made following deductions from the evaluation of interaction of rail wheel.

- With the upsurge in number of cycles, a rise was experienced in traction, both in smooth surfaces and uneven surfaces. Although, surge in smooth surface was prompt that that of uneven surface.
- As measured by ultrasonic transducers there was an effective upsurge in contact stiffness with increase in cyclic rolling. Increases was steeper in case of smooth surface that that of the uneven one.
- Due to cyclic motion on the uneven surface there was a decline observed in RMS roughness coefficient, in case of uneven surface. Although there was no substantial change in case of even surface. There was a slight decline kurtosis.

- An initial model is developed after investigating into the effects of traction characteristics and contact parameters like stiffness.

2.2 Motivation

As studied from the introduction majority of mishaps were due to derailment and derailments are directly related to failure (rolling contact fatigue, adhesive, abrasion, etc.). These wear are due to contact stress intensity developed at the contact patch. As confirmed from above literature, contact patch becomes the utmost parameter on which power transmission and failure is dependent. This high intensity stress becomes crucial to investigate and hence contact parameters are evaluated by FEM in the current study.

2.3 Research Gap

- Most of the work is performed considering half and quarter of the wheel.
- Wheel was considered at rest while simulation in static structural module of Ansys.
- Most of the work is produced without consideration of axle.

CHAPTER 3: PROPOSED METHODOLGY

This project focuses on development and analysis of rail wheel contact problem. Thus evaluation of various results using FEM is done. Furthermore, verification and comparison of results is done using Hertzian Contact Theory. Contact pressure is one of the most important characteristics which are crucial for studying nature of contact patch.

3.1 Hertzian Contact Model

When two bodies are near enough to share a geometry entity at their interface then they are said to be in contact. According to Hertz's theory in contact mechanics when two elastic non-conforming objects are in contact together, then the shape of contact area is in form of a ellipse with *a* and *b* as semi major and semi minor axes.

Heinrich Hertz at the age of twenty four was very interested to identify how does the optical properties of compound lenses are affected when they were applied with force to keep them bonded together. This resulted in his revolutionary work in contact mechanics. He explained the case in which two bodies which are both isotropic and elastic interact with each other when they touch for very small part on their periphery.

Contact pressure distribution in this ellipse shaped contact patch is represented by semi ellipsoid.

Assumptions in Hertzian Theory

- Bodies in contact are considered to be in half spaces which mean contact is very small in size when compared with characteristic radius of the bodies.
- Bodies are isotropic, elastic and homogeneous.
- Continuous and non-Conforming surfaces.

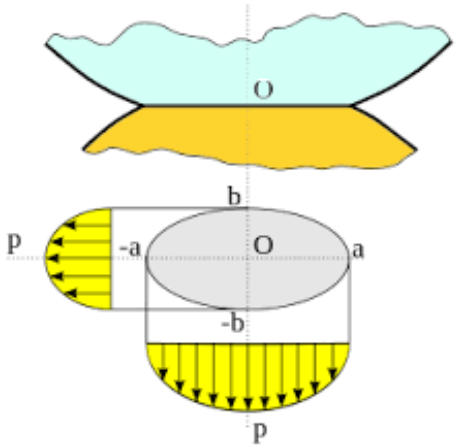

Fig.3.1: Shape of contact patch and pressure distribution

P is given by:

$$P = P_0\sqrt{1 - \frac{x^2}{a^2} - \frac{y^2}{b^2}} \tag{3.1}$$

P_0 is given by:

$$P_0 = 1.5F\left(\frac{1}{ab\pi}\right) \tag{3.2}$$

Where-

P = contact pressure at that point

P_0 = Maximum contact pressure (i.e. when x, y = 0)

a = semi major axis

b = semi minor axis

$$a = m\left[\frac{0.75\pi F(K_1+K_2)}{(A+B)}\right]^{\frac{1}{3}} \tag{3.3}$$

$$b = n\left[\frac{0.75\pi F(K_1+K_2)}{(A+B)}\right]^{\frac{1}{3}} \quad (3.4)$$

Where –

F = Vertical Payload

$$K_n = \frac{1-(\mu_n)^2}{\pi E_n} \quad (3.5)$$

m, n = Hertzian coefficients

Angle	m	n
0.5	61.4	0.102
1	36.89	0.131
1.5	27.48	0.152
2	22.26	0.169
3	16.5	0.196
4	13.31	0.219
6	9.79	0.255
8	7.86	0.285
10	6.604	0.311
20	3.813	0.412
30	2.731	0.493
35	2.397	0.53
40	2.135	0.567
45	1.926	0.604
50	1.754	0.641
55	1.611	0.678
60	1.486	0.717
65	1.378	0.759
70	1.284	0.802
75	1.202	0.846
80	1.128	0.893
85	1.061	0.944
90	1	1
95	0.944	1.061
100	0.893	1.128

Fig. 3.2: Hertzian coefficients

Hertzian Theory is the base for many applications where contact characteristics are required like wear, hardness testing, rail- wheel contact, dental prostheses design, bearings (roller and ball), gear tooth, etc.

Agreeing with the simplest theory of contact mechanics, rail and the rolling wheel is considered to be rigid solids and contact follows Coulomb's friction law. According to this theory, translation and circumferential velocity of wheel are considered to be equal, when tangential force is considered saturated. Transmitted forces are concentrated at a point because of the point contact. Although when frictional losses are considered in the wheel (driver) calculation of stresses (strength), fatigue, vehicle dynamics, wear, etc. becomes difficult.

3.2 Nature and region of contact

According to functional region between rail and wheel contact can have following regions:

- Region A – Contact is present between central zone of wheel tread and middle area of rail head.
- Region B – Contact is present between flange root of wheel and gauge corner of rail.
- Region C – Contact is present between field sides of rail and the wheel.

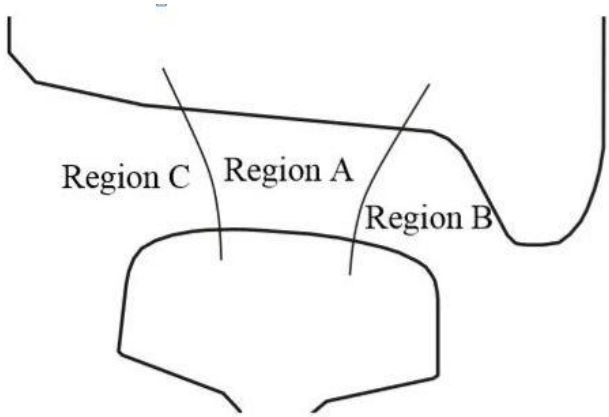

Fig. 3.3: Functional zones in rail wheel contact

Region A

It is the middle region of the wheel tread and the rail crown. Mostly, in this region is where contact occurs, when vehicle is negotiating the gentle curves, tangent track or sharp curves (in steering bogies). Major features in these contacts are:

- Least contact stresses between rail and the wheel
- In stable condition, low creep forces are present
- This zone is optimal for vehicle stability.

Region B

The size of the contact patch formed between rail and the wheel is small. And hence the stress is in the region is generally higher. If there is contact at two points, more wear occurs and flow of material occurs. In case of contact at single point, along with higher contact stresses more creep forces are present too.

This profile has following advantages:

- Shape retention ability of profile is present.
- Support of lubrication is available, because of less specific pressure.
- Neutral conicity (angle between shaft axis and wheel tread profile at the contact region) is present

Region C

It is the contact between field side of the rail and field side of wheel. It is a region of high contact stresses, longitudinal creep forces, incorrect steering sense, etc. Thus, excess flange wear occurs. It generally happens in low rail.

3.3 Solving Contact Problem by FEM

While defining the contact between two surfaces trim tolerance feature is used, after which, all the geometries which are within that tolerance range are considered to be in contact at that time. Gaussian Integration methodology is implemented for calculating the contact patch pressure and area but while employing 2^{nd} order element, oscillations in contact pressure result is observed. Thus, to eradicate such problem so that the results are more conformal to reality we implement Simpson's rule. The oscillating behavior is called chattering effect.

There are fundamentally two algorithms for defining contact between two surfaces

1. Kinematic formulation
2. Penalty algorithm

Kinematic Algorithm

In case of kinematic algorithm, no penetration between two surfaces is present. One of the two surfaces is provided acceleration correction. One of the surfaces (lets name it first surface) is made master and acceleration correction is given, then result is recorded. Subsequently, now the first surface is made slave and then acceleration correction is applied, later reading is again noted. The average two results is taken after multiplying by weights. This process is called 1^{st} correction. While, in 2^{nd} correct similar process is implemented only modification being simple average is taken without the application of weights. Generally, 2^{nd} algorithm is applied for hard surfaces. Therefore, 1^{st} correction has very minute penetration. This is a very strict enforcement.

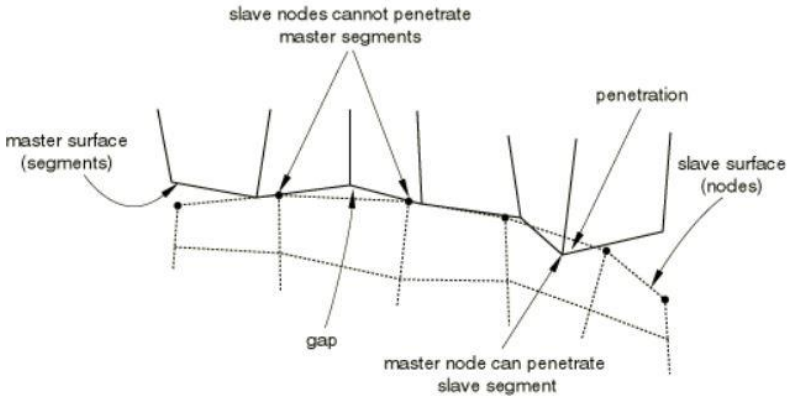

Fig. 3.4: Interacting master and slave at the interface

Penalty Algorithm

In case of Penalty algorithm contact stiffness comes into picture, when two surfaces are in contact.

$$F_n = K_n * x_p \quad (3.6)$$

Where –

F_n = Normal load

K_n = Contact Stiffness

x_p = Penetration

As stiffness is inversely proportional to penetration distance, therefore as K_n approaches infinity, x_p tends to zero, hence increase in accuracy of results. User can control the penetration with by varying K_n value.

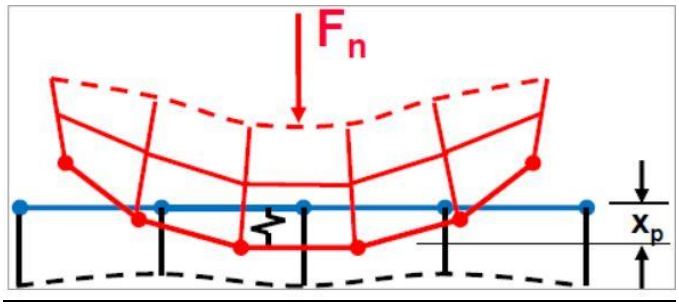

Fig. 3.5: Schematic picture of pure penalty algorithm

There is a special case of penalty algorithm, which is called as Augmented Lagrange, where,

$$F_n = K_n * x_p + \lambda \qquad (3.7)$$

(λ = constant)

Hence we have another parameter (λ) with the assistance of which we can control penetration, along with K_p. Therefore x_p (penetration) becomes less sensitive to K_n(stiffness).

Chattering can be reduced by employing some penetration. Penalty algorithm has less strict enforcement than prior case.

3.3.1 Different types of Contact

In any FEA solver, user has to essentially define the nature of contact, e.g. in case of Ansys contact can be either nonlinear or linear type as described below.

Linear Contact

1. Bonded contact type – Two surfaces are considered to be glued to each other. There exist possibility of no penetration, separation, or sliding between the bonded geometry.

2. No separation – Bodies in contact are restricted to go apart but frictionless sliding is permissible.

Nonlinear

4. Frictionless contact type – Surfaces are permitted go apart and surface are allowed to slide over each other. Penetration of contact and target surfaces is not permitted.
5. Rough contact type – No sliding is possible as the coefficient of friction is considered to be infinite.
6. Frictional contact type – Dependent on user defined coefficient of friction. Bodies are approved to go apart and are unrestricted to slide.

3.3.2 Contact and Target surface designation

Surface assigned as contact has the flexible elements and the surface assigned as target is generally has harder or rigid elements. Therefore, contact (deformable) cannot penetrate target (rigid) elements. Following rules helps in designation of contact and target surfaces.

- When flat or concave face is in contact with convex, then former is made target and later is assigned contact.
- Surface with high discretization is made contact and other is target.
- If a surface envelops the other surface then enveloping surface (bigger) is made target and smaller.

3.3.3 Asymmetric Contact and Symmetric Contact

Asymmetric Contact

All the contact elements are on the surface designated as Contact whereas each target element is on Target surface. In easy words, it is the interaction between rigid and flexible surfaces. It is more efficient methodology than symmetric contact.

Symmetric Contact

Both Contact and Target surfaces are having target and contact elements. In other words, it is the interaction between two flexible surfaces. Result elucidation is challenging. Contact pressure results are mean of pressure of the two surfaces. When using this approach with coarse mesh on both the surfaces, a lot of computational resources and time are needed, hence expensive than prior approach.

3.3.4 Direct Solver vs. Iterative Solver

Direct solver

In case of direct solver, exact results are produced by pre-multiplying of inversed stiffness matrix with force matrix. The shortcomings faced in this methodology is that sometimes matrices are sparse matrices which means that a lot of elements are zeros therefore lot of computational time and resources are wasted in solving integers getting multiplied with zero. Other disadvantages include lot of time wasted in inverting and then multiplying large matrices. LU decomposition, Gaussian elimination techniques, etc. are used to evaluate results.

$$F = Ku \tag{3.8}$$

$$K^{-1}F = u \tag{3.9}$$

Iterative Solver

In iterative solver methodology, initial guess is made (say u_0) and then solution is progressed and next better value u_1 is found then u_2 and so on till

$$Ku_n - F = 0 \tag{3.10}$$

Where n = 0, 1, 2, 3, ……

Hence, this solving technique provides approximate result.

3.4 Development of CAD Model

CAD model of rail and the wheel was developed in Solidworks 2016. It was then converted into step file. Step file format is a neutral format which assists as common currency for importing and exporting CAD files. Later, this file will be imported as geometry in Ansys Workbench.

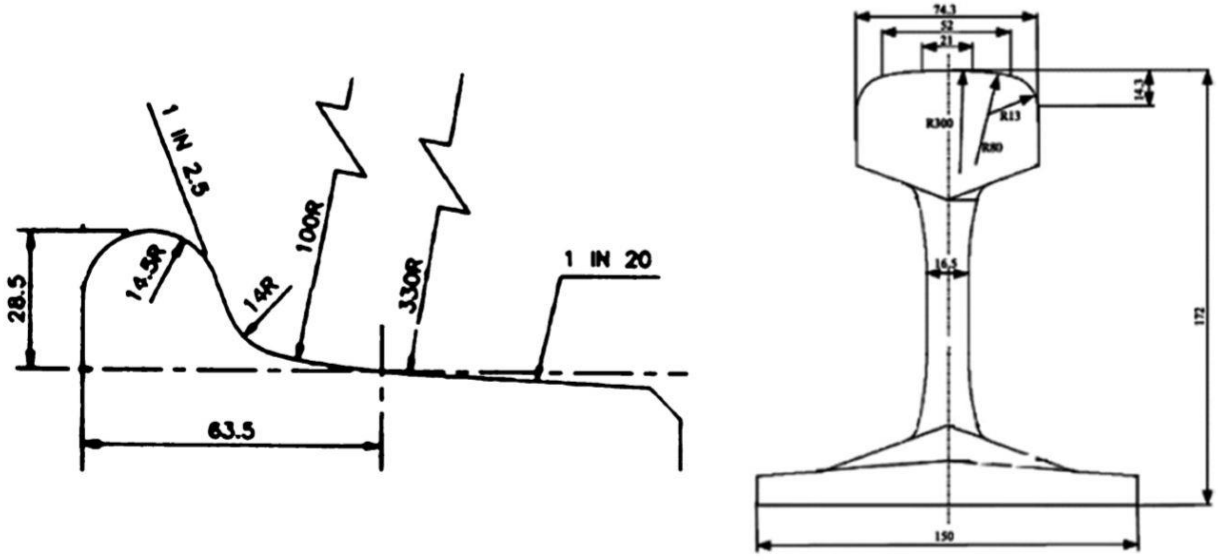

Fig. 3.6: Schematic diagram of rail and wheel profiles

The Standard Rail profile (UIC60) was sketched on front plane and extruded by 1 m. The corresponding wheel can be chosen with radius ranging from 460mm (passenger) to 500mm (freight). All the parts were assembled in assembly module of Solidworks. The assembly was the converted in step file.

3.5 Ansys Workbench 18.2

Following is the snapshot of workbench where static structural module is selected and dragged to project schematic (region in white).

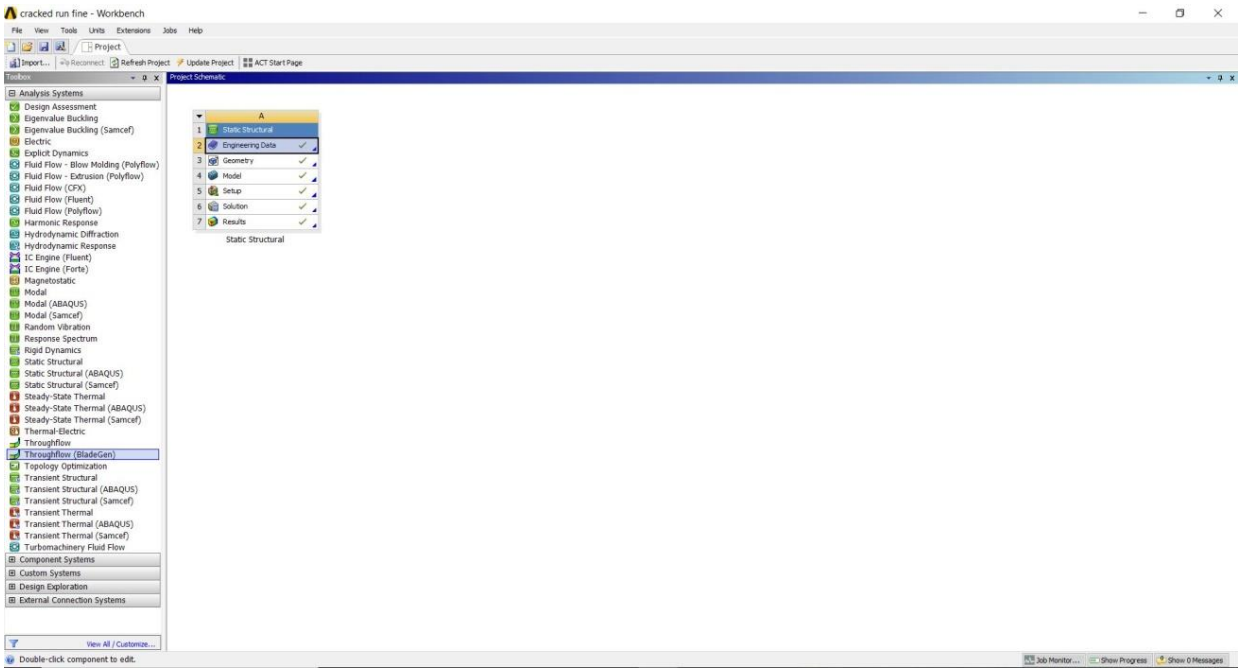

Fig. 3.7: Ansys Workbench with static Structural module

3.5.1 Material properties

By double clicking on Engineering Data tab from the module, a new window is opened and structural steel with appropriate values of E and μ are added. Majority of the focus was on Young's modulus of elasticity and poisson's ratio which were taken as 210 GPa and 0.3 respectively. Following material properties were defined for a rail, wheel and the axle. This process adds the material to library, which can be accessed from Mechanical Module.

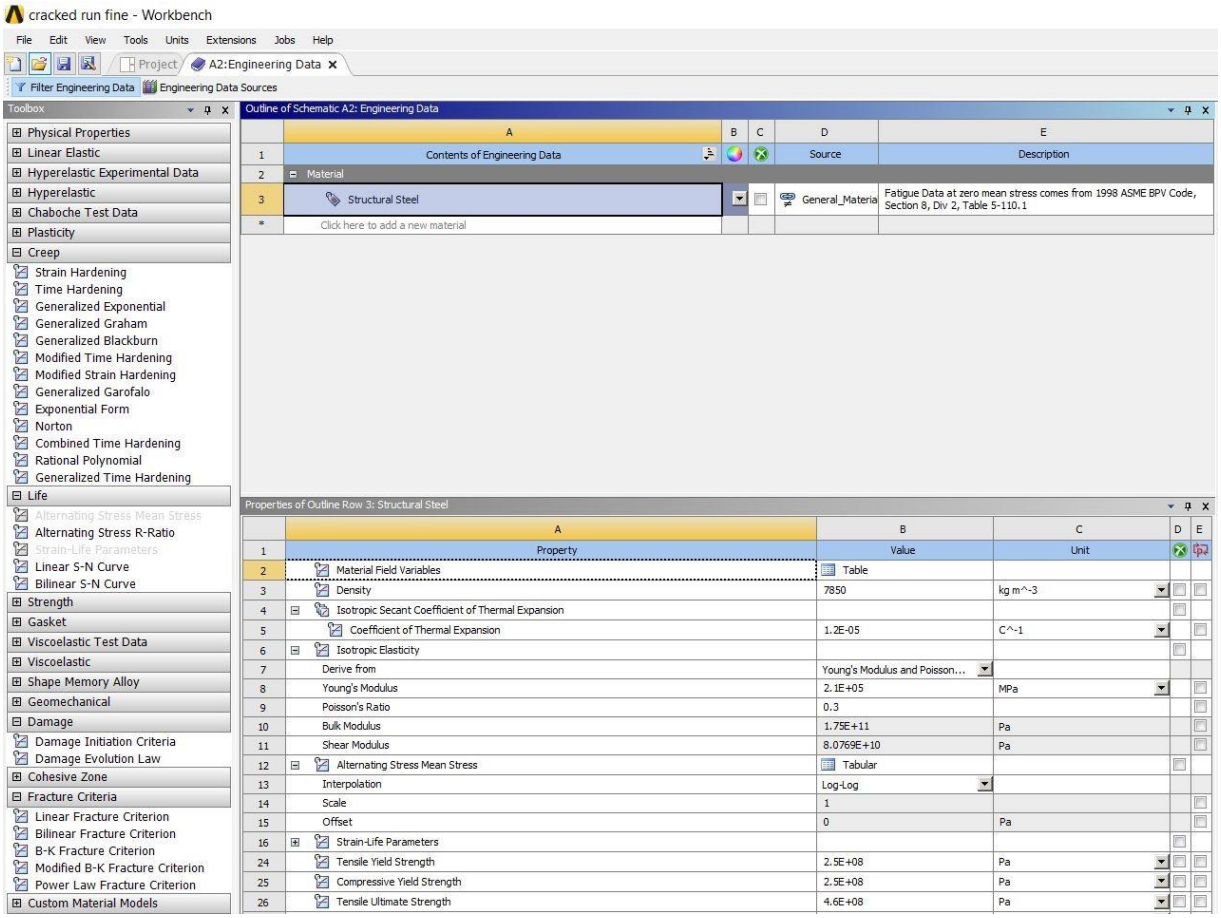

Fig. 3.8 Description of engineering data and material properties

3.5.2 Model

Double click on Model tab in the workbench to open mechanical module. On the left side project tree different selections are made in different sub-divisions of simulation process, to perform the analysis. Application of boundary condition, Loads, definition of connections, coordinate axis, setting up of analysis, visualization of results, etc. are done here.

3.5.3 Material assignment

For assigning the material to the geometry, click on each geometry from the project tree and in 'detail' window, select assignment to structural steel.

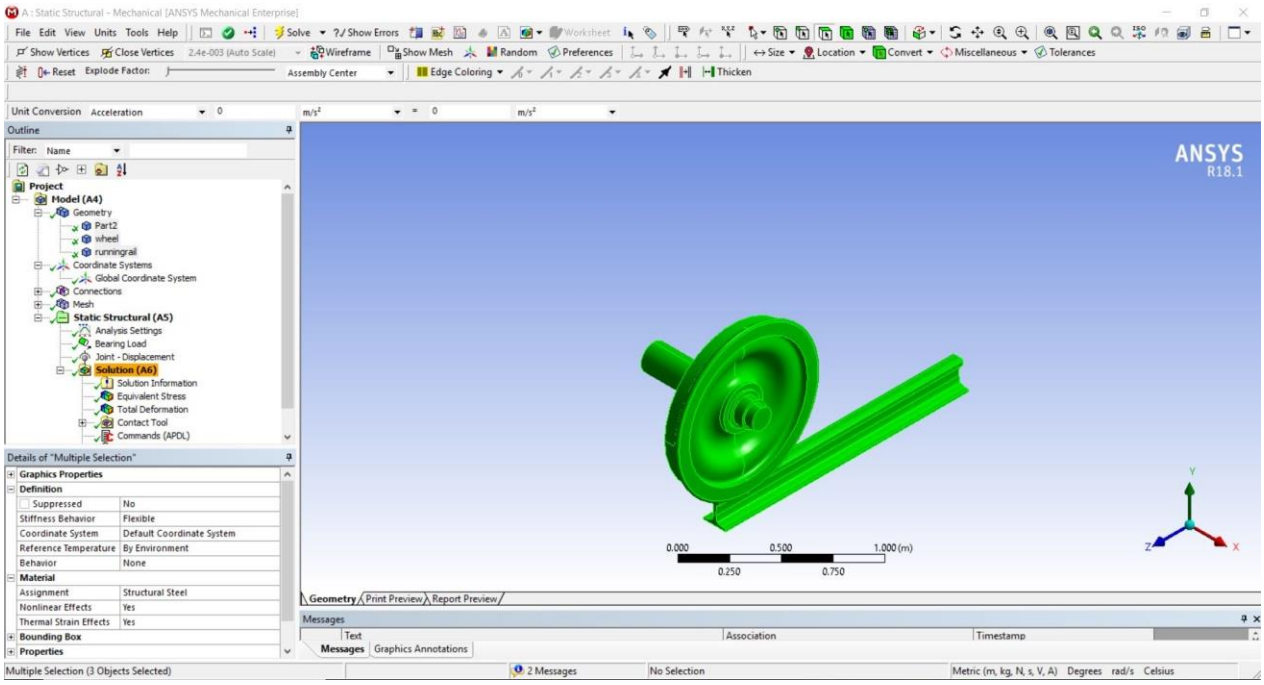

Fig. 3.9 Material assignment to CAD geometry

3.5.4 Contact Initialization in the FEA Solver

Contact was initialized at two locations i.e. in between (i) rail and the wheel; (ii) wheel and the axle. Both the contacts are nonlinear in nature and hence, interface at rail and the wheel was assigned frictional contact with coefficient of friction μ = 0.3. Moreover, contact interface between axle and the wheel was defined as frictionless contact. As the shape of wheel at the contact is in convex form, hence it is selected as Contact Body and rail is relatively flat in therefore it is selected as Target body. Target body is generally shown in blue and contact body is colored as red. Trim Tolerance is initialized as 5.9952×10^{-3}. Pure Penalty method is selected as the contact algorithm.

3.5.5 Contact between rail and the wheel

For defining contact, in project tree select connection then Contact, expand contact tab. Select contact tab for rail wheel interaction. Now in 'Detail' box apply contact body as wheel (red) and target body as rail (blue). Input definition type as frictional with coefficient of friction 0.3.

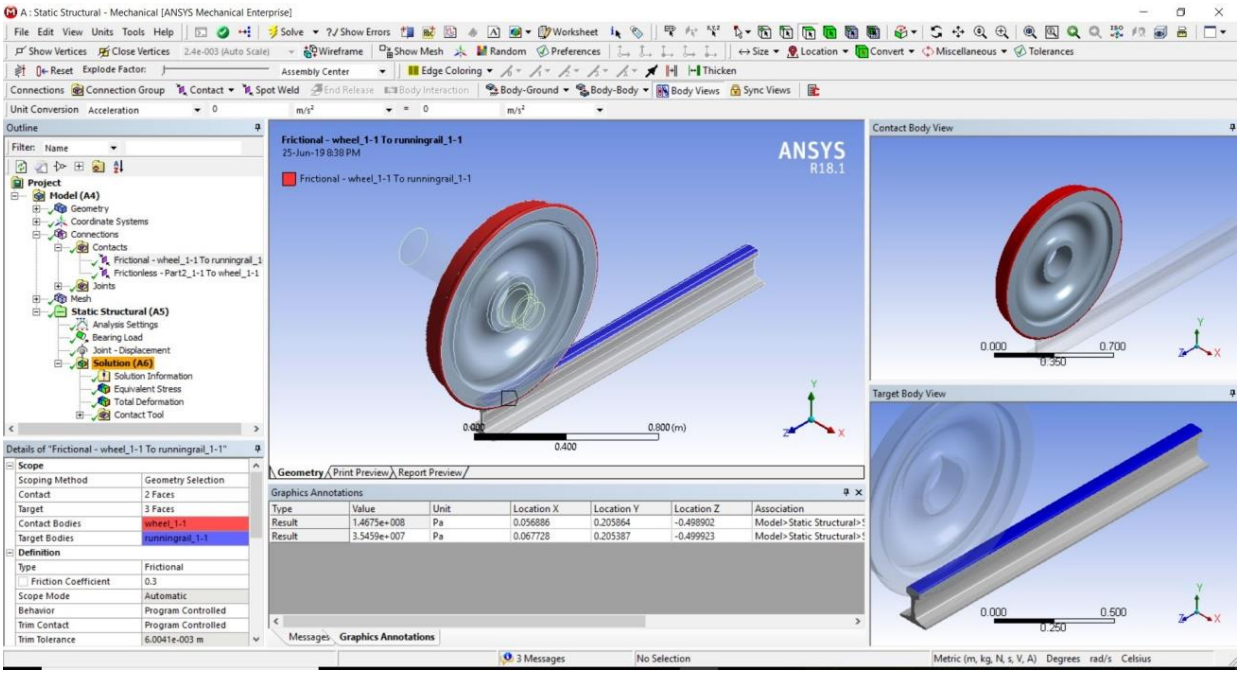

Fig. 3.10: Wheel is defined as contact body and rail as target body in rail wheel interface

3.5.6 Contact between axle and the wheel

Contact between wheel and the hub is initialized as frictionless behavior that means sliding is possible without loss in energy. Provision of axle in the model, makes the work closer to reality. Here the periphery of the wheel is made target whereas, the outer surface of the axle is made contact. Therefore, larger surface is target body and smaller surface is contact body.

From the project tree, select the contact between axle and the wheel. Go to ‘Detail’ box and select axle as contact and wheel as target. Enter the definition type as frictionless.

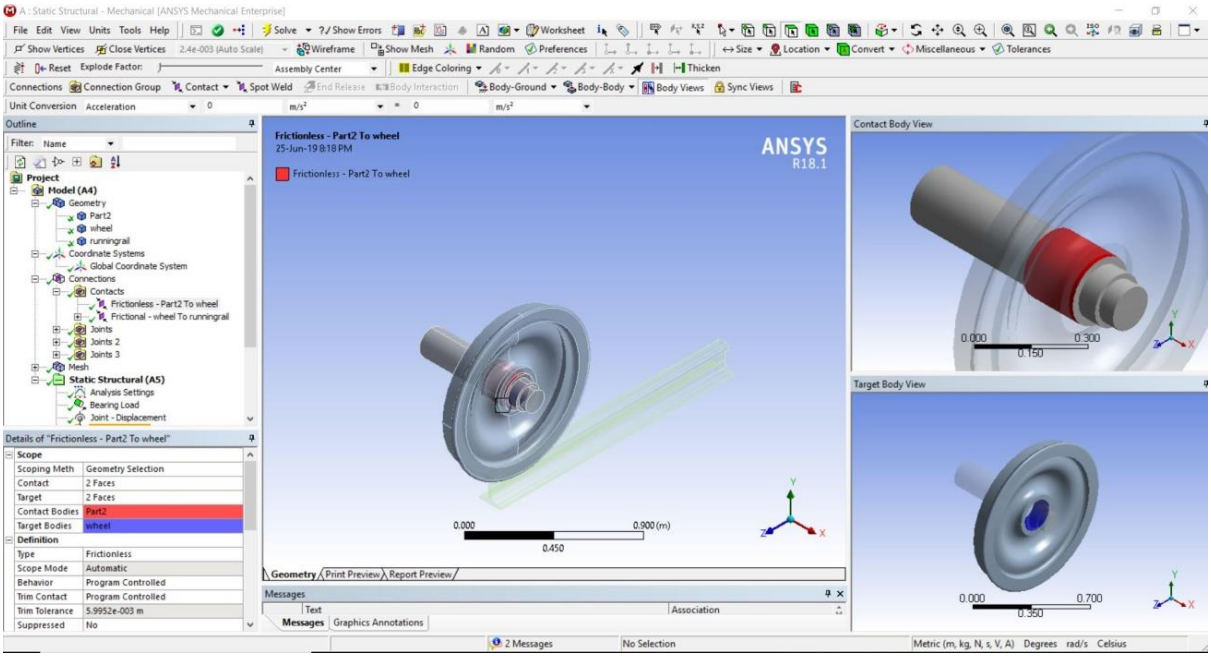

Fig. 3.11: Axle surface is defined as contact body and wheel bearing zone as target body at wheel axle interface

3.5.7 Boundary Condition Definition

Model was furnished with three vital boundary conditions, as shown in figures below. Boundary conditions were defined in form of joint definition in the connection sub group.

1. Initializing the rail lateral surface as fixed with respect to ground.

Right click on ‘Connections’ and insert joints. In join select fixed w.r.t. ground joint. In ‘Detail’ box of joint apply prompt is shown. Select the surfaces to fix and then click on apply in ‘Detail’ prompt.

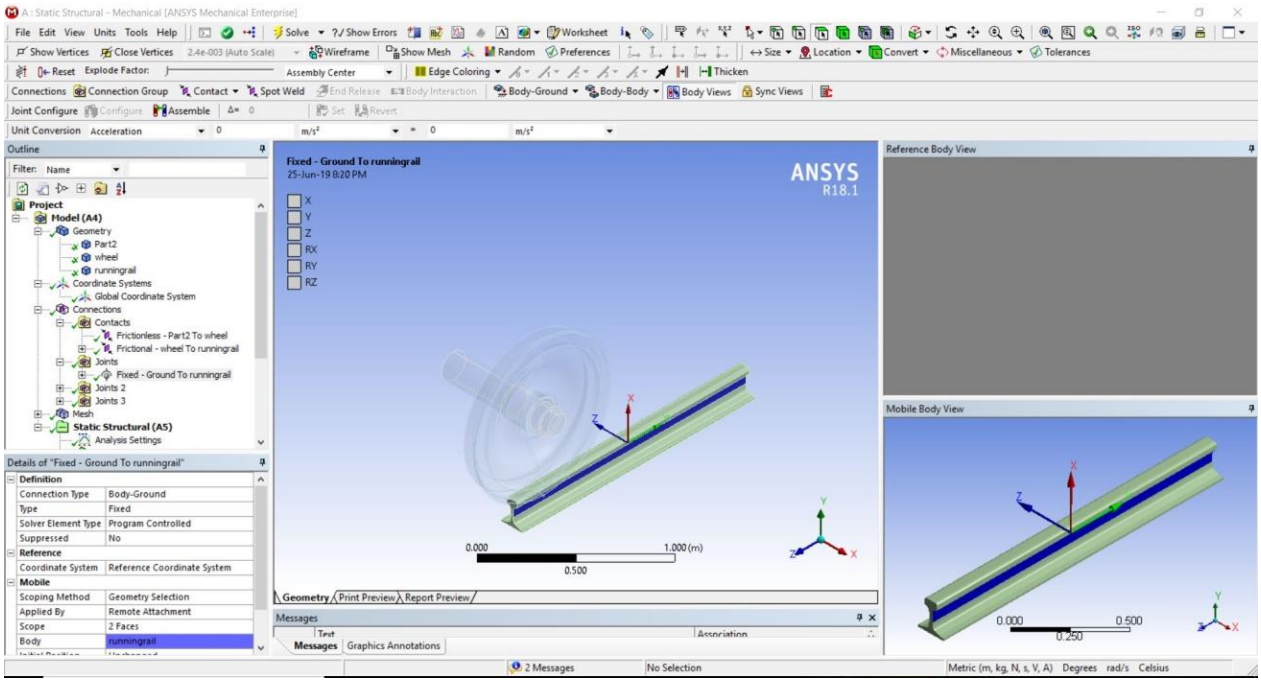

Fig. 3.12: Fixed boundary condition in rail

2. Apply boundary condition by adding translational joint in connection tab. Translation joint w.r.t. ground is added to axle surface inside the bearing location of wheel, which is prompted as apply in 'Detail' box. Select proper coordinate axis as shown in figure below.

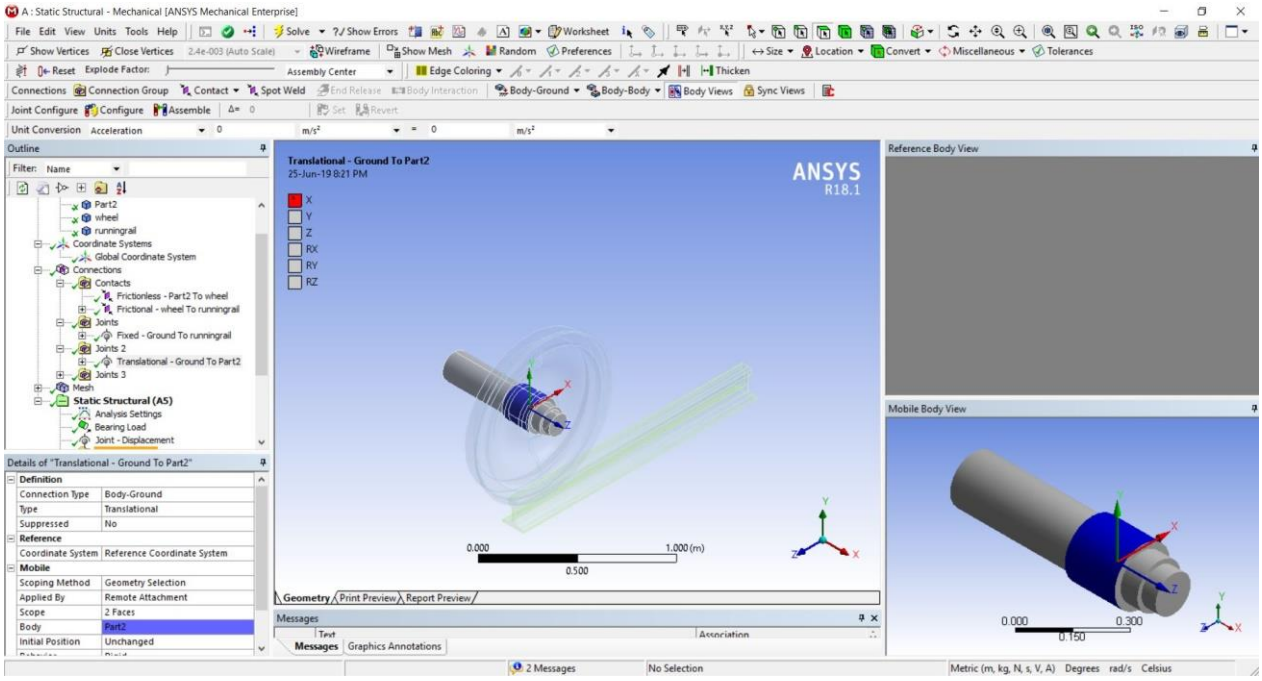

Fig. 3.13: Axle surface was given freedom to move in x- direction w.r.t. ground

3. Applying planar join to flat surface on the wheel. This boundary condition allows the motion of wheel in x and y coordinates and rotation about z-axis. For applying this, right click on connection to enter planar joint w.r.t. ground and in 'Detail' box select the geometry against the apply prompt. Correct the coordinate axis such that axis of rotation is along z-axis by expanding joint tab and making z as principal axis in 'Detail' box.

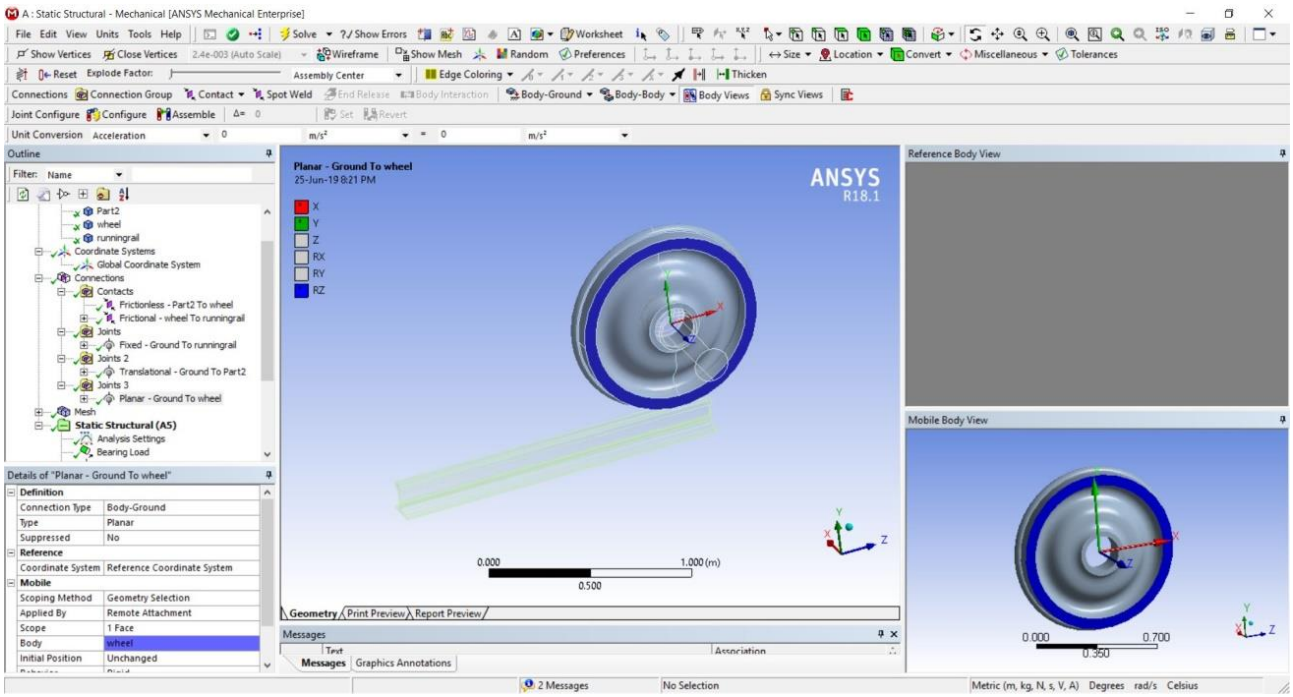

Fig. 3.14: Wheel was allowed to move in x and y direction and freedom to rotate with z as reference.

3.5.8 Discretization of model

Model was discretized with face sizing by selecting rail and wheel interacting surface. Hence it was given Tet mesh with face sizing of 7 mm. rest of the bodies were given fine relevance setting to have good quality mesh with growth rate of 1.2. A body colored mesh was generated with minimum edge length of 0.0004476 m. Mesh Adaptiveness was selected as on with initial seeding size dependent on assembly.

The reason for the provision of very fine face mesh was that to avoid rebound of surfaces when load is applied. As the more number of elements are good at energy absorption during impacts hence smaller rebound is observed. Because of this feature

steady state values are reached faster and healthy contact remains between rail and the wheel.

Click on mesh option from the project tree then, right click to insert ‘sizing’ option. Select the contact surfaces from the geometry (physical model), which are then given 7 mm element size from the ‘Detail’ box.

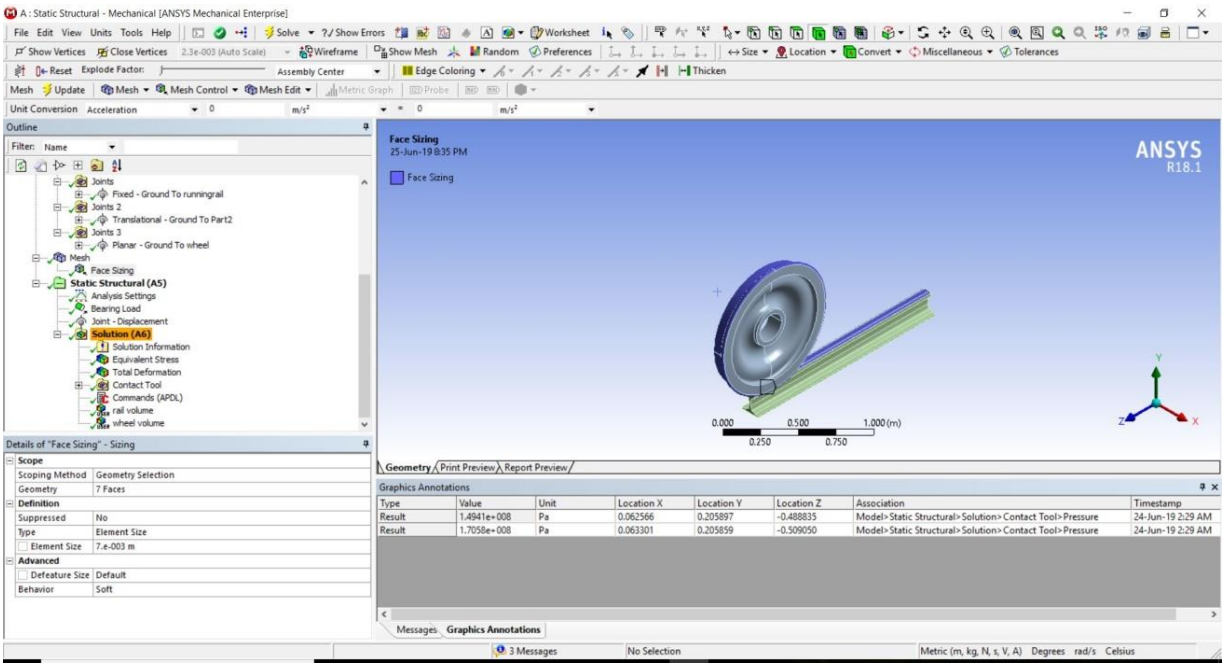

Fig. 3.15: Face selection in progress for reefing the mesh size

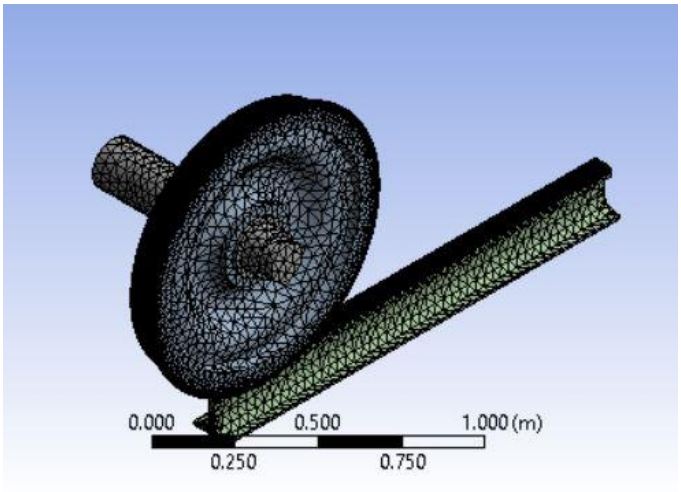

Fig. 3.16: Discretized model with very fine mesh at interacting surface of rail and wheel

3.5.9 Analysis Settings

Correct analysis settings plays important role, when accurate results are desired. Click on Analysis Settings tab from the project tree. In the 'Detail' box, enter no. of steps as 5, current step number as 5 and step end time as 5 second. Switch on auto time stepping. Select 'define by' as time. Minimum time step is entered as 0.001 second and maximum time step as 0.1 second. Direct Solver is selected to have accurate results and large deflection as on. Make weak spring setting as off and program control pivot checking.

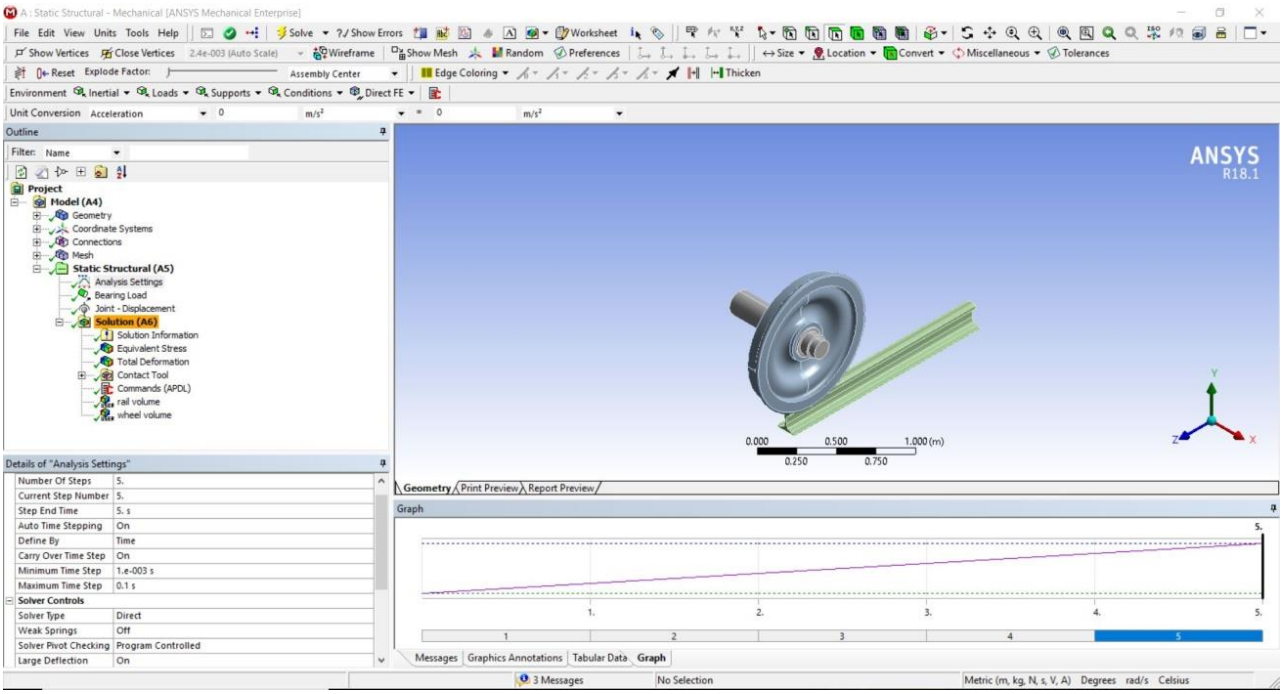

Fig. 3.17 Selection of analysis Settings in 'Detail' box

3.5.10. Setting up loads

a. Bearing Load

Rail wheel was given a downward vertical bearing load at bearing location. A load of 80000 tons act on eight wheels, which means a total of 10 ton weight (dead weight of wagon and payload) act on each wheel. Hence load of 100000 N is applied at the bearing location with consideration of worst case scenario.

Right click on A5 and add bearing load. In 'Detail' box select apply button after selecting the bearing location. (Select axle from tree and press F9 to hide axle and have

proper visualization of bearing location.) Select ‘define by’ as ‘component’ and enter 100000 N, in negative y-direction.

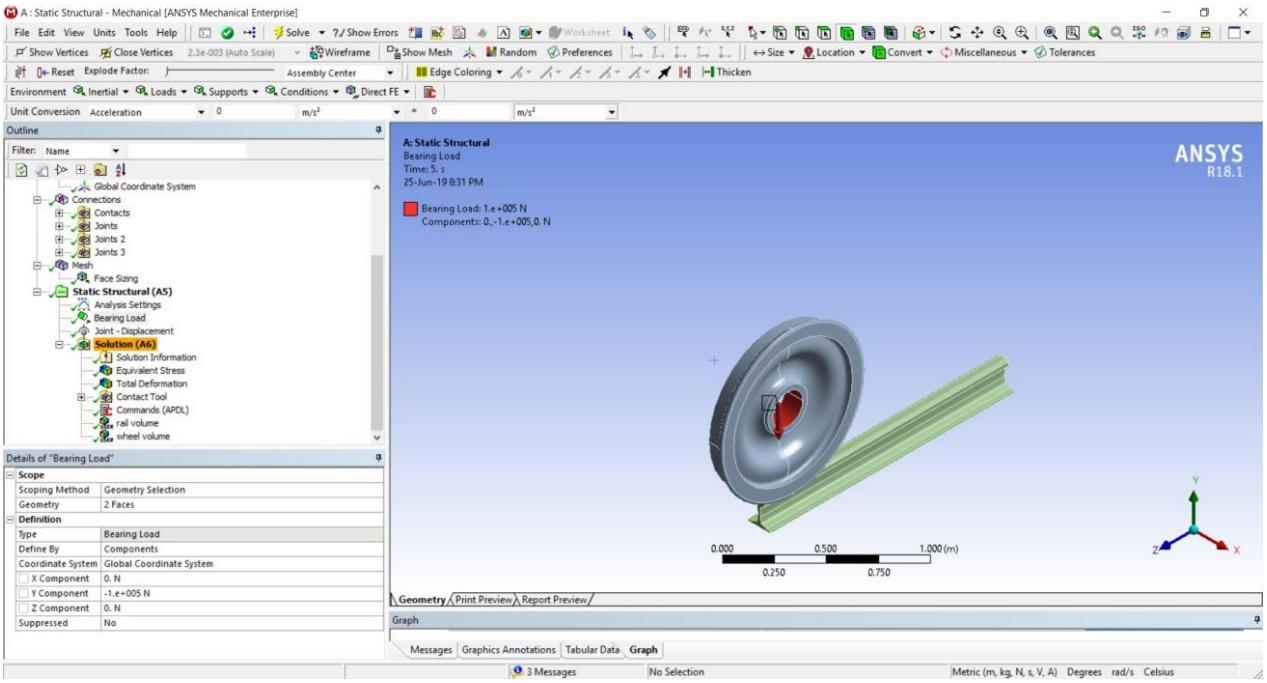

Fig. 3.18: Bearing load application in downward direction

b. Joint load

A joint load was applied at the axle of displacement 0.5 m. This load was assigned in tabular for varying linearly with time.

Table 3.1: Application of displacement to the axle w.r.t. time

S. No.	Time (s)	Displacement (m)
1.	0	0
2.	1	0.1
3.	2	0.2
4.	3	0.3
5.	4	0.4
6.	5	0.5

Right click in ‘A5’ to insert joint load. In ‘Detail’ box, select translation joint. In ‘definition type’ select the ‘displacement’ option. Magnitude of displacement is entered in tabular form as the table above.

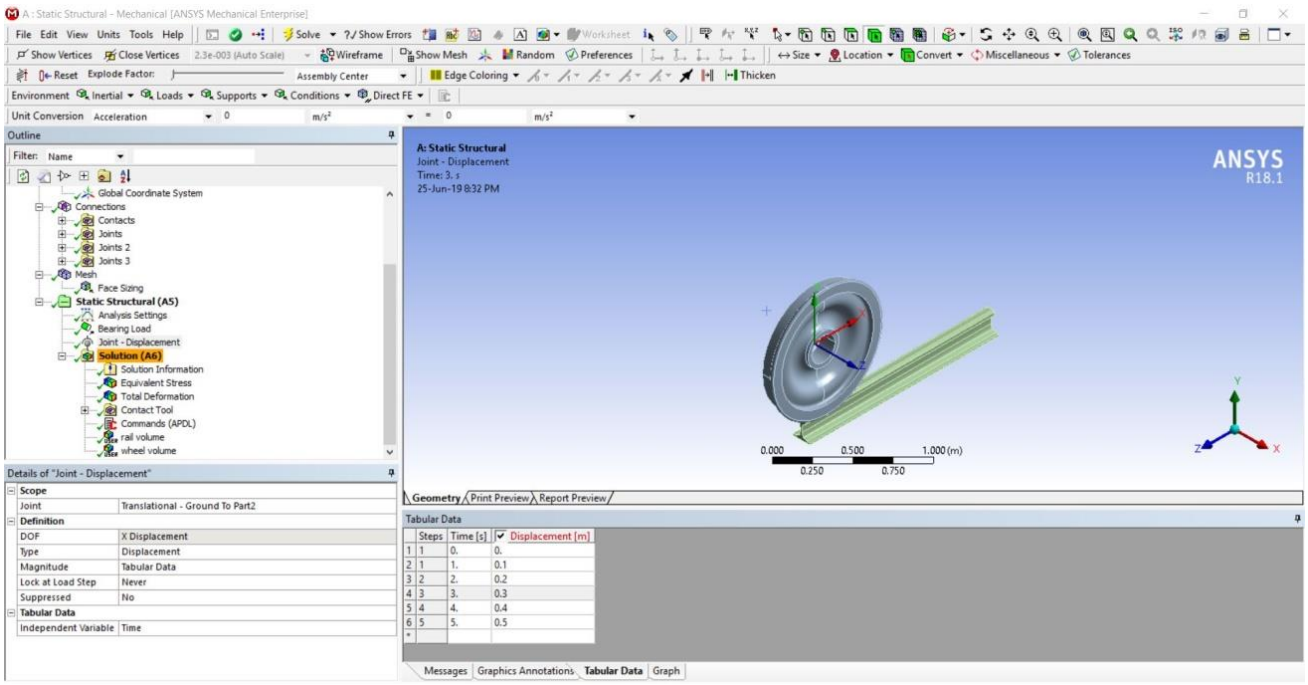

Fig. 3.19: Joint load application in positive x- direction

Click on Solve button and insert all required parameters (Von Mises stress, deformation, contact tools, etc.) in ‘A6’.

3.6 Archard Wear

When two surfaces interact in such a way that rubbing action takes place, then there is a possibility of material removal from less harder material. Wear depends on material properties both mechanical and chemical and also on dynamic conditions like velocities and forces. The wear volume is calculated according to Archard’s expression –

$$V_a = k\frac{W}{H}L$$

$$A_r = \frac{W}{H}$$

Where

A_r = Contact Area [m^2]

W = Applied Load [N]

H = Hardness (softer material) [Pa]

L = Sliding distance [m]

K = Wear Coefficient (Proportionality Constant)

If the value of K is small, it means wear is has occurred due to small asperities in contact.

Specific Wear Rate (k) is defined by following expression

$$k = \frac{V}{(W)(L)}$$

Where

L = Sliding length [mm]

V = Wear Volume [mm^3]

K = wear rate or specific wear rate [mm^3/ (N – mm)]

Let's consider a sliding asperity which spherical in shape, having plastic properties and is able to completely deform.

Therefore,

Area of contact $A_r = \pi a^2$ [a = asperity radius]

Hardness (H) of the soft material is equal to mean constant pressure

$$H = \frac{W}{\pi a^2}$$

Volume (V) of debris formed when asperity of radius *a* slides a length of 2a

$$V = \frac{2\pi a^3}{3}$$

Wear volume per unit sliding length (U)

$$U = \frac{K\pi a^2}{3}$$

From above equation we get,

$$\pi a^2 = \frac{W}{H}$$

$$U = \frac{K * W}{3H}$$

Introducing k,

$$k = \frac{K}{3}$$

Total wear volume (V) when sliding length is L

$$V = U * L$$

Putting the value of U we get,

$$V = k\frac{W}{H}L$$

3.7 Modeling Wear at contact Interface

Archard wear can be included into the simulation at the interface of contact body for that an Ansys APDL command is incorporated in to the contact definition. Wear simulation is exhibited as reduction of pressure. Wear on rail is selected as the body.

After wearing off, there is a requirement of re-meshing of the surface for that adaptive meshing is done using nladaptive command.

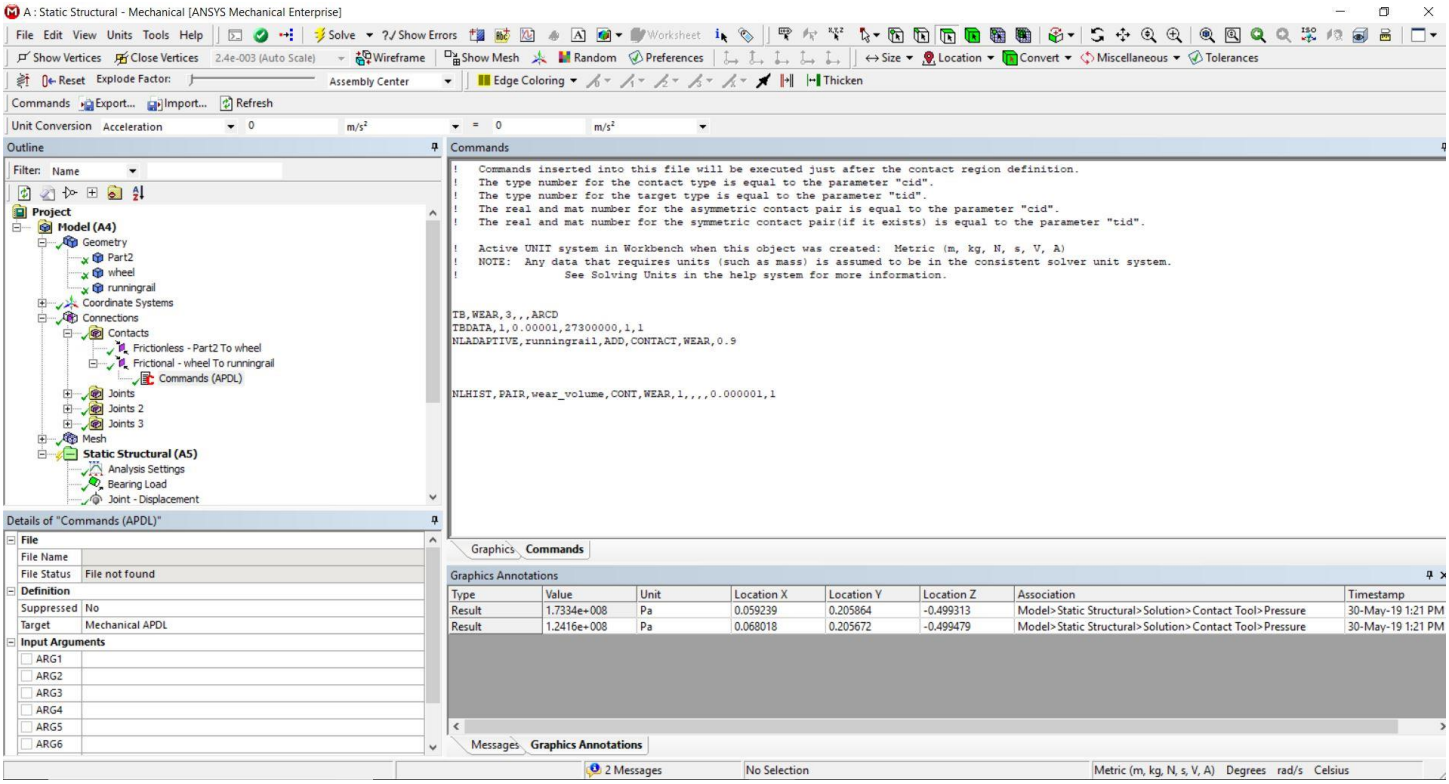

Fig. 3.20: Wear Sub-Routine initialization in Ansys APDL

Wear coefficient, harness of material, velocity exponent and pressure exponent are the required values to be input into the subroutine. In the current case TBDATA command is used to incorporate these values.

$K = 10^{-5}$

H = 27300000 Pa

$m_v = 1$; $n_p = 1$

3.8 Verification of the model using Hertzian Method

As we know the dimensions of interacting geometry, therefore

R_{11} = 488.4mm, (Radius of Wheel)

R_{12} = 458mm, (Radius of wheel w.r.t. rail)

R_{21} = ∞, (Radius of straight line)

R_{22} = 300mm (general value for rail wheel interface)

φ = 1

Putting above values in below relations

$$A + B = 0.5\left(\frac{1}{R_{11}} + \frac{1}{R_{12}} + \frac{1}{R_{21}} + \frac{1}{R_{22}}\right) \quad (3.11)$$

$$B - A = 0.5[\left(\frac{1}{R_{11}} - \frac{1}{R_{12}}\right) + \left(\frac{1}{R_{22}} - \frac{1}{R_{21}}\right)^2 + \left(\frac{1}{R_{11}} - \frac{1}{R_{12}}\right)\left(\frac{1}{R_{22}} - \frac{1}{R_{21}}\right) Cos2\varphi]^{0.5} \quad (3.12)$$

We get,

A+B = 3.7821 * 10^{-3} mm^{-1} and B-A = 1.598714 * 10^{-3} mm^{-1}

$$\text{Cos } \theta = \frac{B-A}{A+B} \quad (3.13)$$

We get, θ = 64.9947, which is almost equal to 65 deg ,

Hence, value of Hertzian coefficients

m = 1.378, n = 0.759

We can evaluate semi-major and minor axis by the following equations

$$a = m\left[\frac{0.75\pi F(K_1+K_2)}{(A+B)}\right]^{\frac{1}{3}} \quad (3.14)$$

$$b = n\left[\frac{0.75\pi F(K_1+K_2)}{(A+B)}\right]^{\frac{1}{3}} \quad (3.15)$$

Where, $K_n = \frac{1-(\mu_n)^2}{\pi E_n}$

F = 100000 N; $\mu_1 = \mu_2 = 0.3$

$E_1 = E_2 = 210000$ MPa

We get,

$K_1 = K_2 = 1.3793*10^{-6}$ MPa^{-1}

J = 5.5597

a = 7.66134 mm; b = 4.2198 mm

3.9 Verification of the contact pressure using Hertzian Method

As described by Hertzian method maximum pressure is given by following equation:

$$P_0 = 1.5F\left(\frac{1}{ab\pi}\right) \quad (3.16)$$

Putting: F = 100000 N

a = 7.66134 mm; b = 4.2198 mm

We get maximum pressure P_0 = 1476.8785 MPa

CHAPTER 4: BENCHMARK PROBLEM OF CYLINDER ON PLATE

4.1 Problem Description

The cylinders in this example have a radius of 254 mm and are elastic, with Young's modulus of 206 GPa and Poisson's ratio of 0.3. Smooth contact (no friction) is assumed.

The contact area remains small compared to the radius of the cylinders, so the vertical displacements along the diametric chord of the cylinder that is parallel to the contact plane are almost uniform. This, together with the symmetry of the problem, requires only one-quarter of one cylinder to be modeled. Displacements are prescribed on the diametric cut parallel to the rigid plane to load the problem. For this example the nodes along the diametric cut are displaced vertically down by 10.16 mm (0.4 in). The total load per unit length of the cylinder can be obtained by summing the corresponding reaction forces on the cylinder or equivalently as the reaction force on the rigid body reference node.

Contact forces will be generated on the bottom surface of the cylinder due to the displacement boundary condition. The contact forces generated must be able to produce the same displacement when applied as a uniformly distributed load on the top surface of the cylinder.

4.4 Displacement Boundary condition

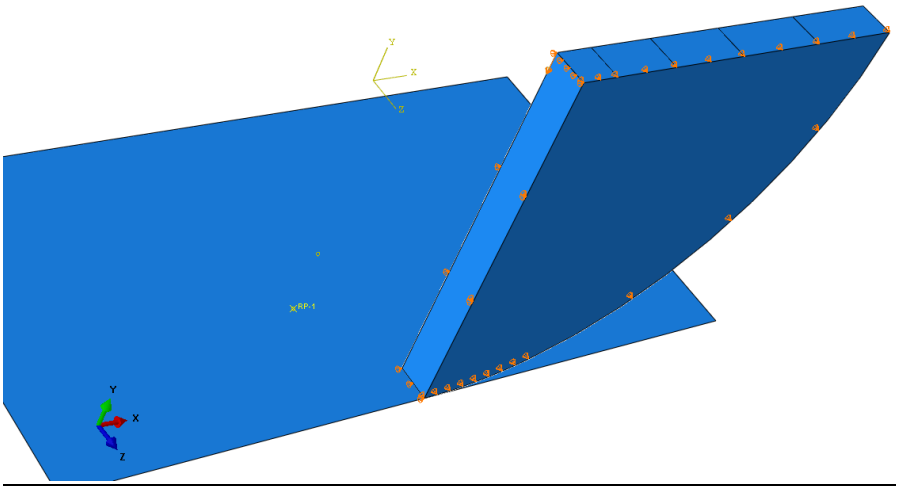

Fig. 4.1: The diametric cut is displaced vertically down by 10.16 mm

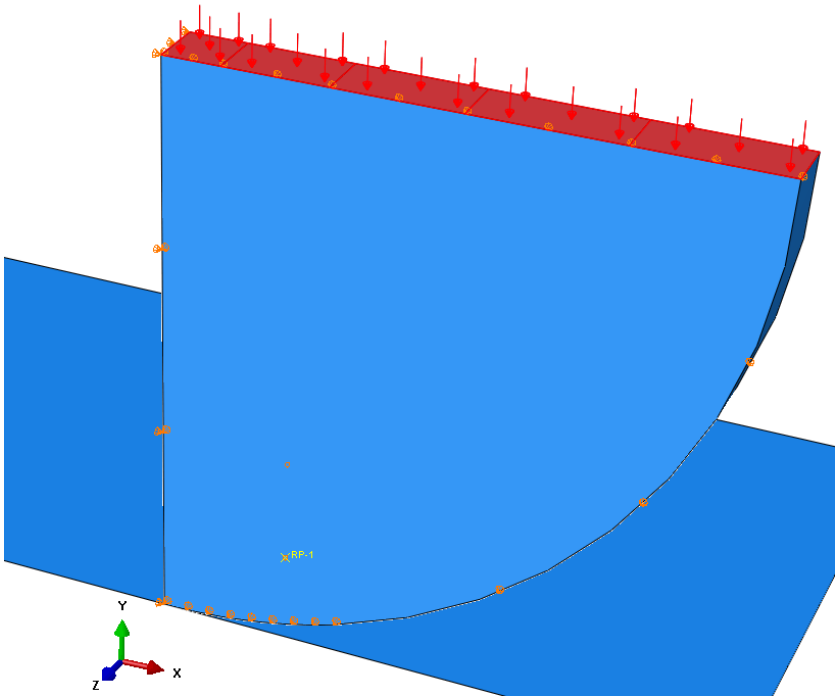

Fig. 4.2: Ramp load of 312057 N is applied

A uniformly distributed load equal in magnitude to the contact force generated in the previous analysis will be applied on the top surface of the cylinder

4.3 Contact conditions

Because of symmetry, the contact problem can be modeled as a deformable cylinder being pressed against a flat, rigid surface. Therefore, two contact surfaces are required: one (the slave surface) on the deformable cylinder and the other (the master surface) on the rigid body.

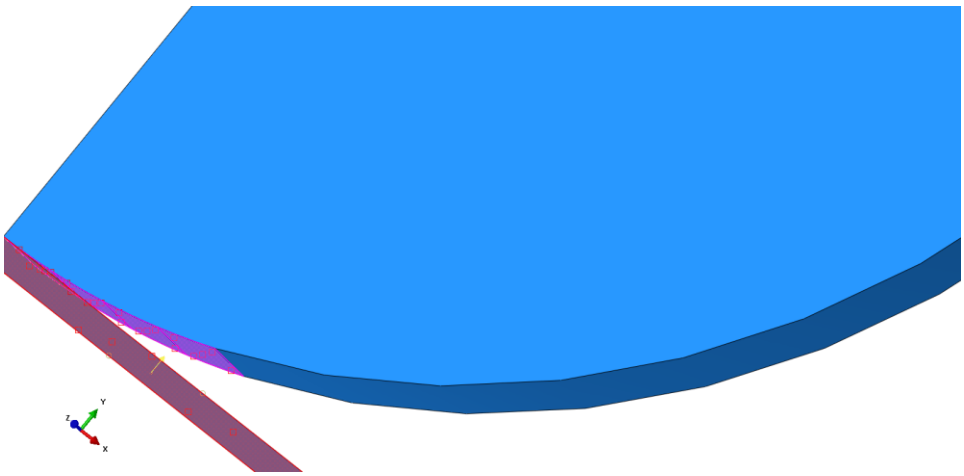

Fig. 4.3: Assigning of master and slave contact condition

By default, FEA solver uses a finite-sliding contact formulation for modeling the interaction between contact pairs. The contacting surfaces undergo negligible sliding relative to each other, which makes this problem a candidate for the small-sliding contact formulation. Discretization method will be taken as Node to Surface.

4.4 Mesh elements

The bulk of the cylinder is modeled in Abaqus/Standard with 16 20-node bricks; the remaining four elements that abut the surface where contact may occur are modeled with element type C3D27, which is a brick element that allows a variable number of nodes. This element is intended particularly for three-dimensional contact analysis. Element type C3D27 always has at least 21 nodes: the corner nodes, the mid-edge nodes, and one node at the element's centroid.

4.5 Results

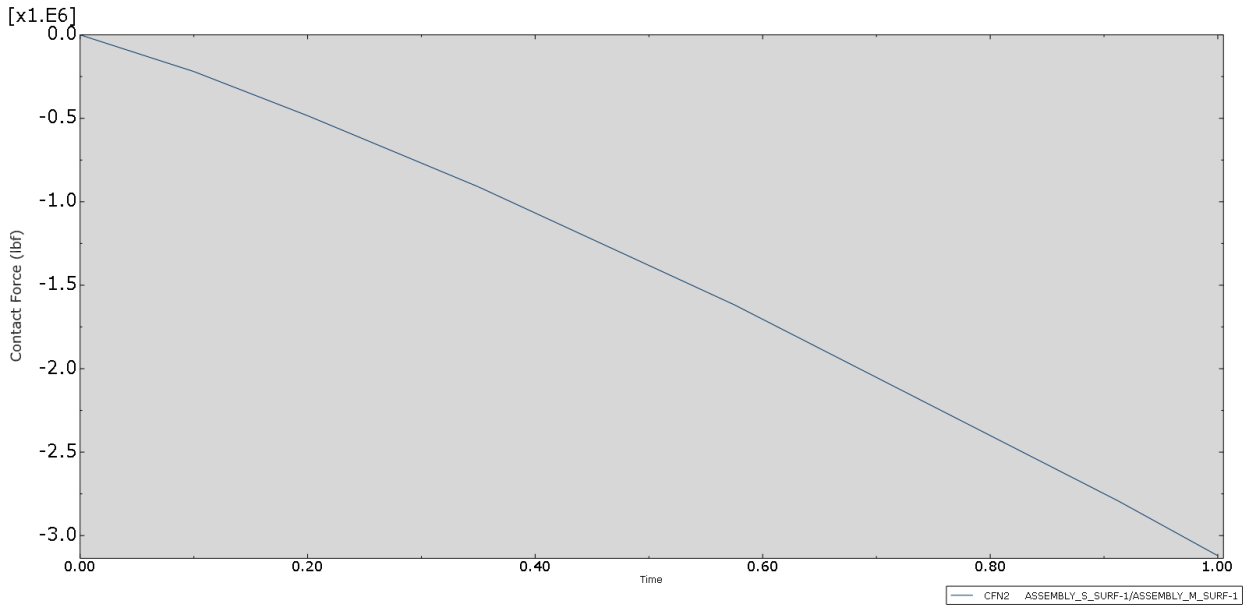

Fig 4.4: Plot of contact forces due to contact stress in y-direction

Table 4.1: Contact Forces variation with time

Time at in sec (x-axis)	Contact Force in N (y-axis)
0	0
0.1	-219771
0.2	-484392
0.35	-910244
0.575	-1.61714E+006
0.9125	-2.79258E+006
1	-3.12057E+006

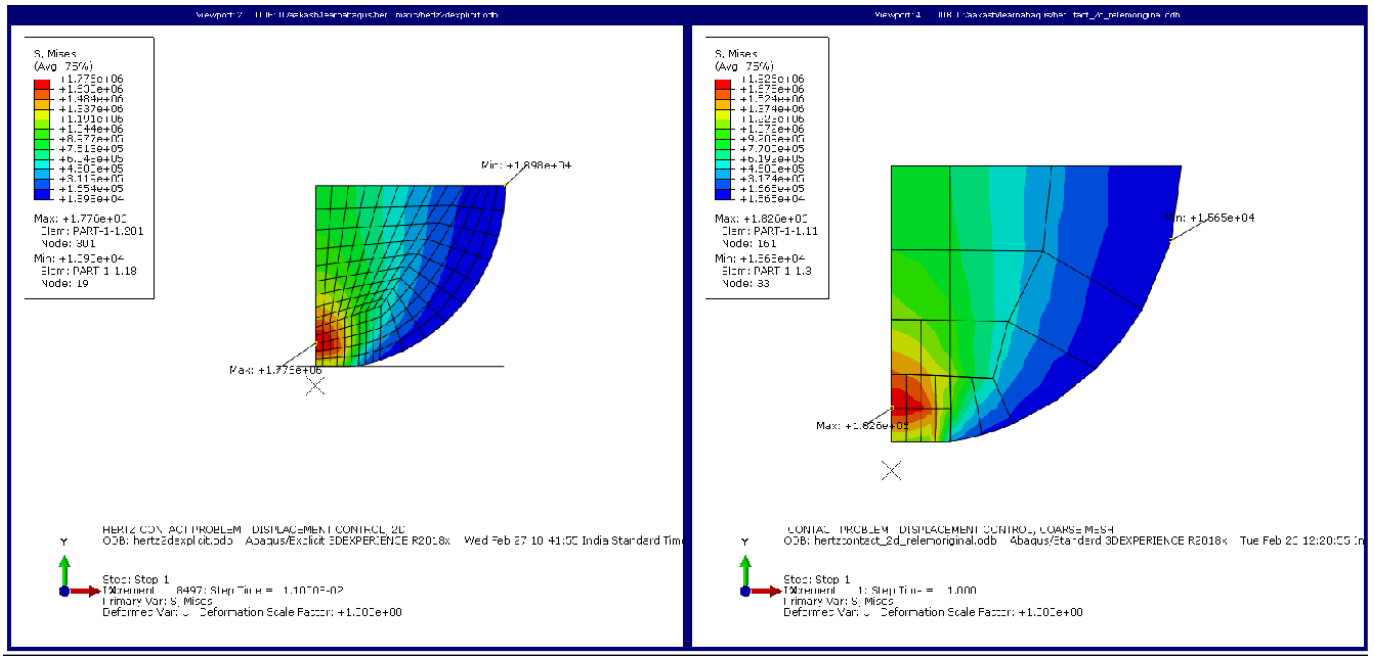

Fig 4.5: Comparison of Von Mises Stresses of Different Mesh Size

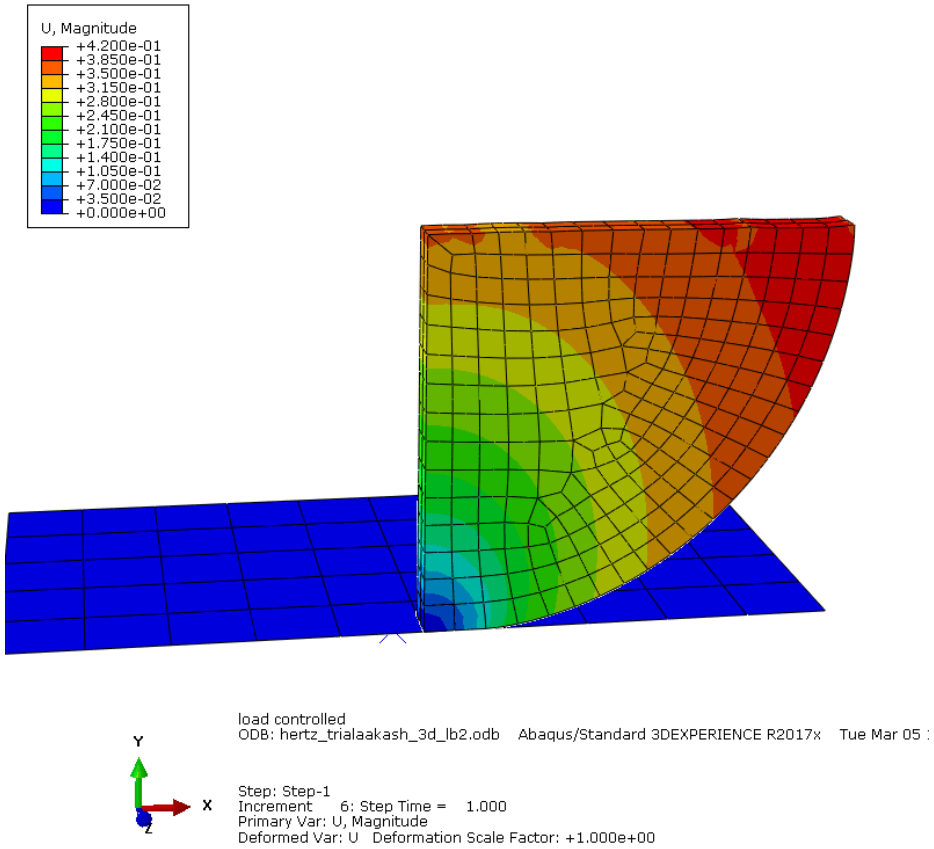

Fig. 4.6: Equivalent Deformation

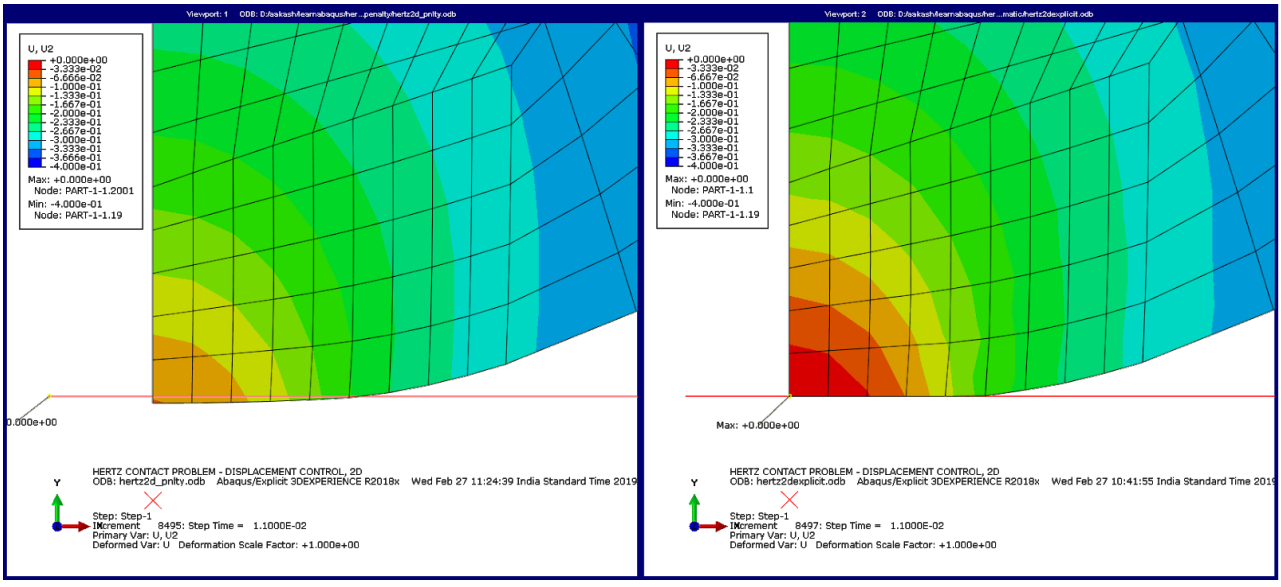

Fig. 4.7: Comparison of contact pressure for penalty (left) and kinematic algorithm (right)

4.6 Mesh Convergence

Following mesh convergence shows results are independent of mesh size.

Table 4.2: Mesh Convergence

s no.	mesh size (mm)	number of elements	number of nodes	Contact Pressure (MPa)	Von Mises stress (Mpa)
1	18	532	2784	256.72	375089
2	12	968	5146	257.825	394286
3	6	6328	30363	254.849	1.68379E+007
4	2.5	5964	24946	256.4	1.052E007
5	1.25	15712	61794	252.175	1.38E007

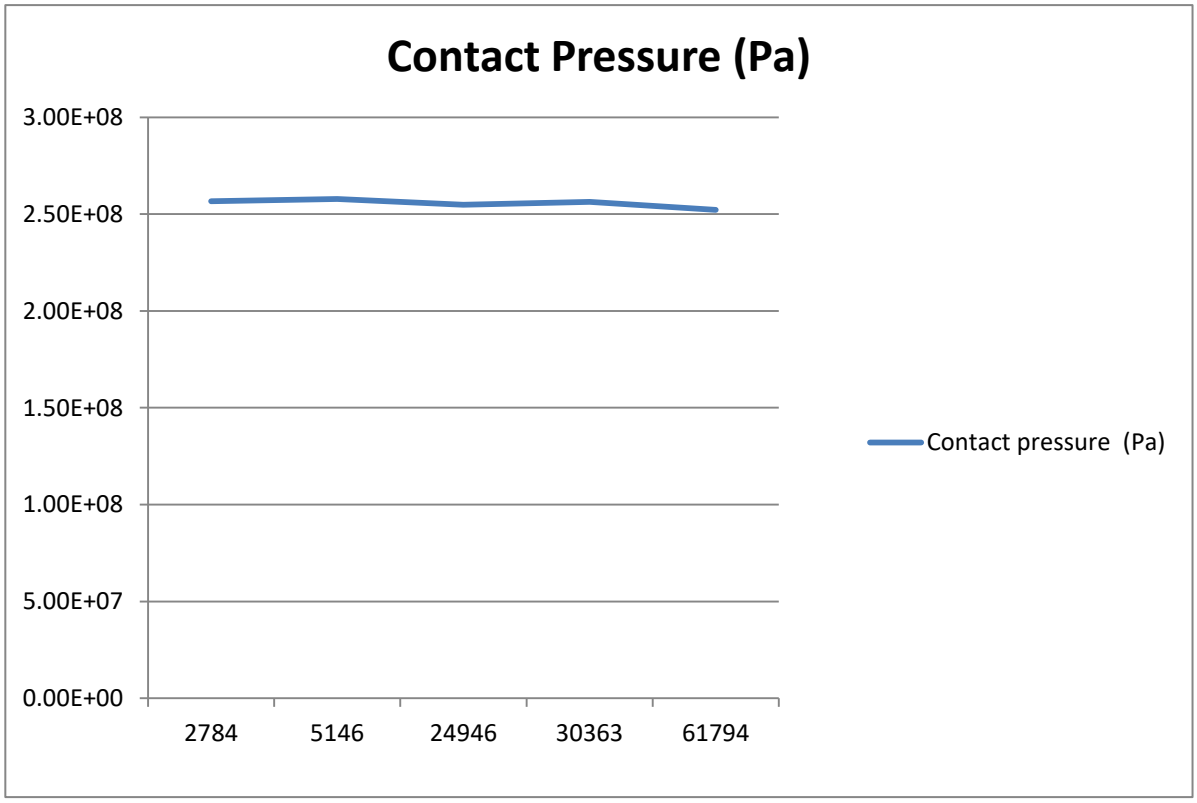

Fig. 4.8: Variation of contact Pressure w.r.t. no. of nodes

4.7 Verification of the model using Hertzian Method

As we know the dimensions of interacting geometry, therefore

R_{11} = 254mm, (Radius of cylinder)

$R_{12} = \infty$ (Radius of straight line)

$R_{21} = \infty$ (Radius of straight line)

$R_{22} = \infty$ (Radius of flat plate)

$\varphi = 1$

Putting above values in below relations

$$A + B = 0.5\left(\frac{1}{R_{11}} + \frac{1}{R_{12}} + \frac{1}{R_{21}} + \frac{1}{R_{22}}\right) \quad (4.1)$$

$$B - A = 0.5[\left(\frac{1}{R_{11}} - \frac{1}{R_{12}}\right)^2 + \left(\frac{1}{R_{22}} - \frac{1}{R_{21}}\right)^2 + \left(\frac{1}{R_{11}} - \frac{1}{R_{12}}\right)\left(\frac{1}{R_{22}} - \frac{1}{R_{21}}\right) Cos2\varphi]^{0.5} \quad (4.2)$$

We get,

$A+B = 1.9685 * 10^{-3}\ mm^{-1}$ and $B-A = 1.9685 * 10^{-3}\ mm^{-1}$

$$\text{Cos } \theta = \frac{B-A}{A+B} \quad (4.3)$$

We get, $\theta = 0$,

Hence, value of Hertzian coefficients

m = 62.19, n = 0.102

We can evaluate semi-major and minor axis by the following equations

$$a = m\left[\frac{0.75\pi F(K_1+K_2)}{(A+B)}\right]^{\frac{1}{3}} \quad (4.4)$$

$$b = n\left[\frac{0.75\pi F(K_1+K_2)}{(A+B)}\right]^{\frac{1}{3}} \quad (4.5)$$

Where,

$$K_n = \frac{1-(\mu_n)^2}{\pi E_n}$$

F = 312057 N

$\mu_1 = 0.3$

$E_1 = 206000$MPa

$E_2 = \infty$

We get,

$K_1 = 1.406126 * 10^{-6}$ MPa^{-1}

$K_2 = 0$ MPa^{-1}

J = 10.088

a = 627.390 mm

b = 1.0208 mm

4.8 Verification of the contact pressure using Hertzian Method

As described by Hertzian method maximum pressure is given by following equation:

$$P_0 = 1.5F\left(\frac{1}{ab\pi}\right) \quad (4.6)$$

Putting: F = 312057 N

a = 627.390 mm; b = 1.0208 mm

We get maximum pressure $P_0 = 232.62$ MPa

4.9 Percentage error in solution

Table 4.3: Comparison of Benchmark problem Results with Hertz contact theory

	Hertz Contact Model	FEM
Contact Pressure	232.62	252.175

Percentage Error in solution = $\frac{252.175-232.62}{252.175} * 100$

= 7.75 %

CHAPTER 5: RESULTS

5.1 Analytical Results

As it is investigated from the analytical solution of Hertz Method, contact pressure and contact patch size is evaluated and is equal to:

Semi major axis ‘a’ = 7.66134 mm

Semi minor axis ‘b’ = 4.2198 mm

Maximum Contact pressure ‘P_0’ = 1476.8785 MPa

Following figures shows the results of various contact parameters solved by FEM tool Ansys 18.1.

5.2 Computational Results

FEA solver Ansys 18.1 was used to compute results for contact problem. Following are the evaluated results for rail wheel contact and their plots showing variation with time.

5.2.1 Equivalent Von Mises Stress

Maximum equivalent stress has been evaluated in the wheel rail setup and is show in figure 4.1. Maximum Von Mises stress are found to be lesser than contact pressure which was around 1300 MPa. Maximum Von Mises stresses attains steady state value after first second of simulation run.

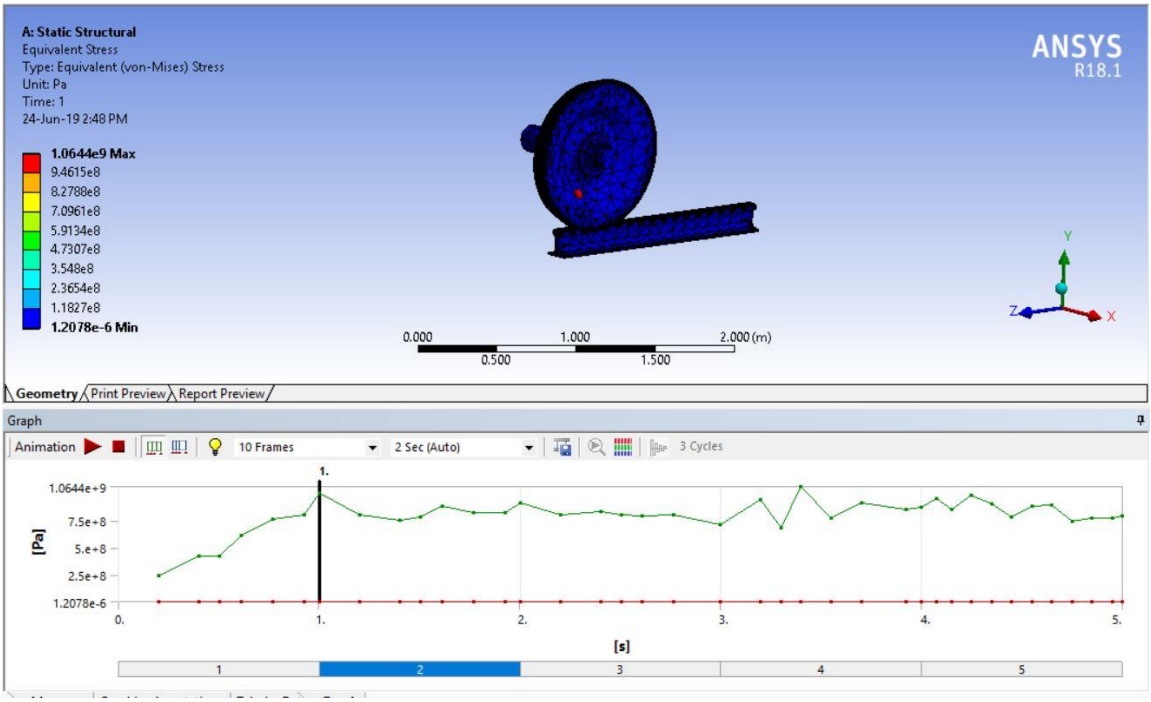

Fig. 5.1: Variation of Equivalent Von Mises stress w.r.t. time

5.2.2 Contact Pressure

Contact patch is in the form of ellipse as described by the Hertzian theory. As the region of patch is very small, the pressure values are very high. After reaching the steady state region the pressure variation are very low as shown by fig. 4.3.

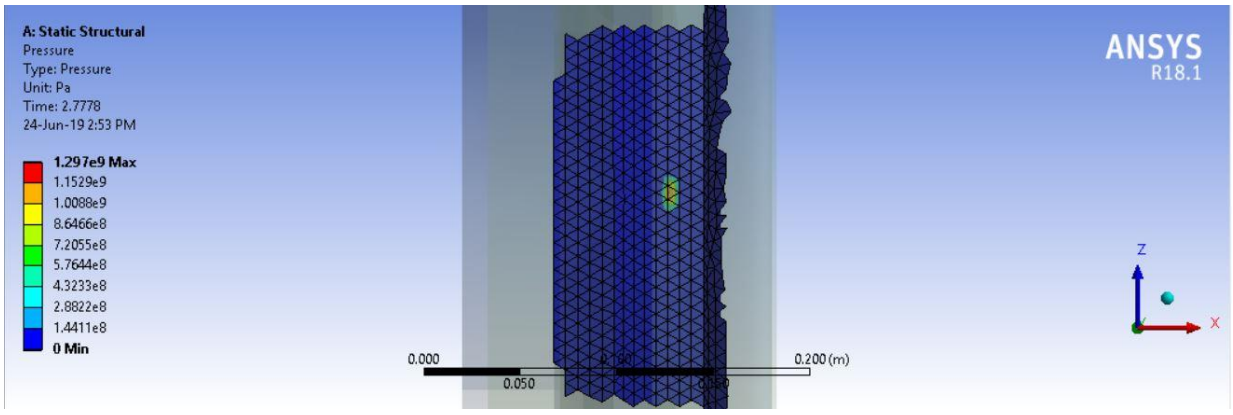

Fig. 5.2: Contact patch formation at the interface (without wear)

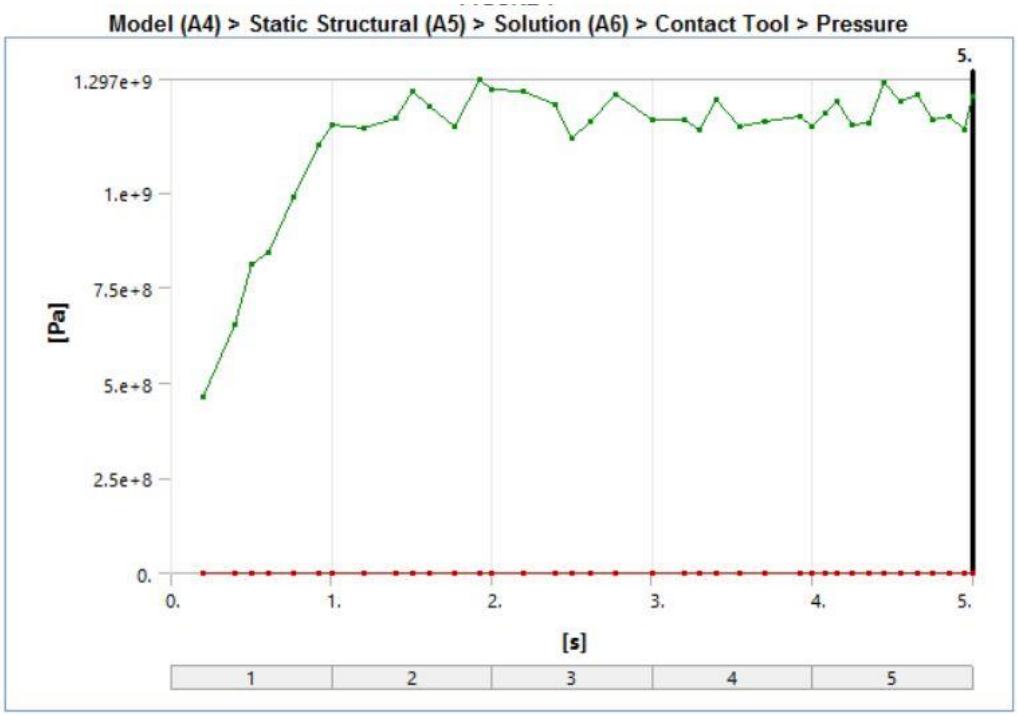

Fig. 5.3: variation of contact Pressure w.r.t. time (without wear)

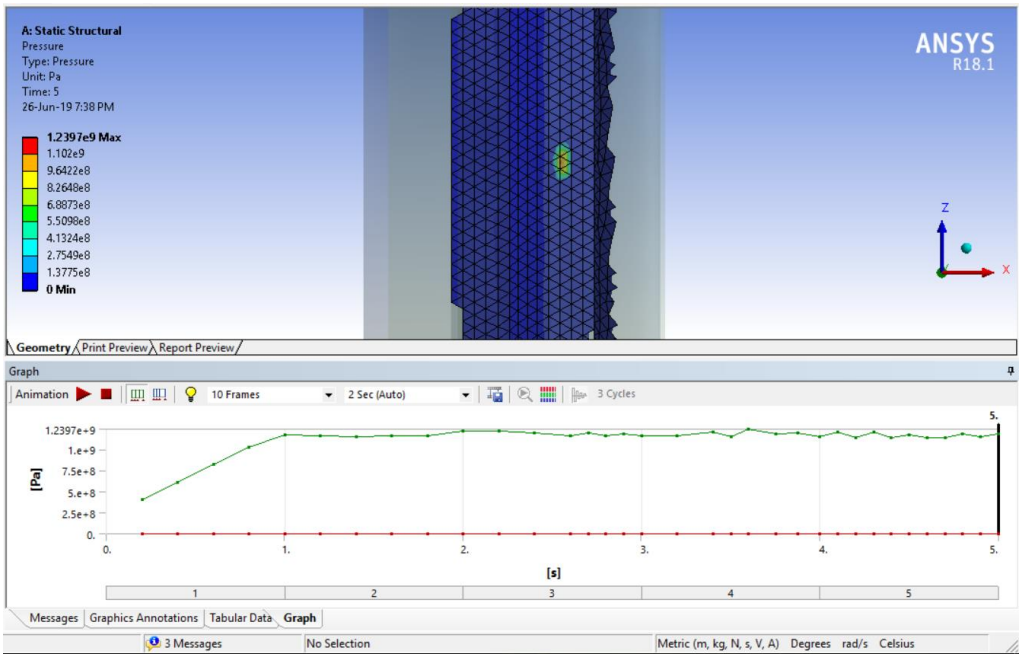

Fig. 5.4: Contact patch formation at the interface (with wear)

5.2.3. Contact Patch size

Contact patch size is also dependent upon wear. When surfaces in contact interact, due to wear surfaces becomes more conformal and hence area of contact patch increases. Therefore, semi major axis and semi minor axis size also increase.

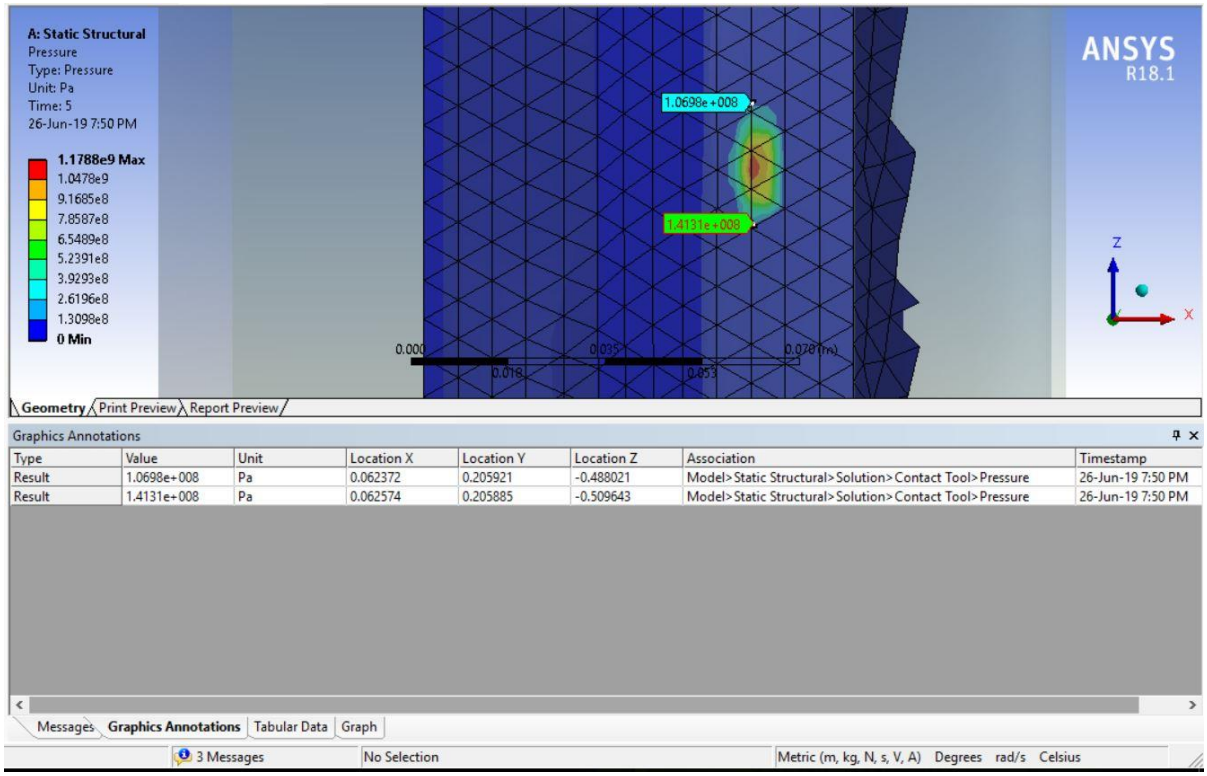

Fig. 5.5: Semi major axis ‘a’ (without wear)

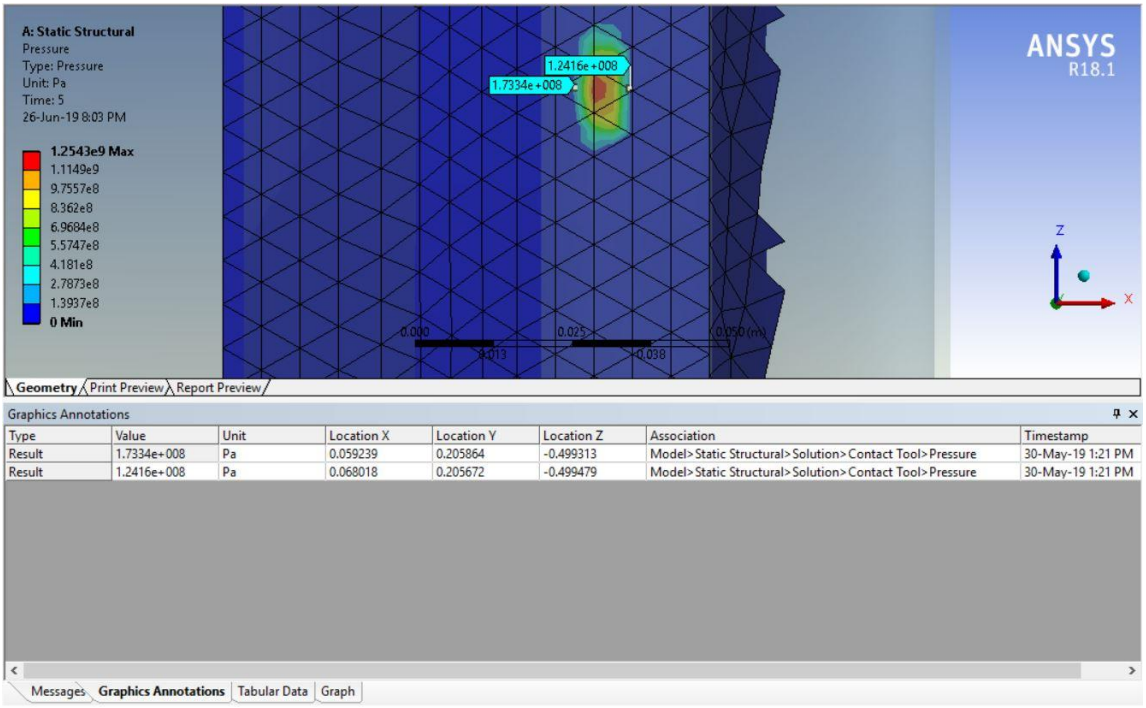

Type	Value	Unit	Location X	Location Y	Location Z	Association	Timestamp
Result	1.7334e+008	Pa	0.059239	0.205864	-0.499313	Model>Static Structural>Solution>Contact Tool>Pressure	30-May-19 1:21 PM
Result	1.2416e+008	Pa	0.068018	0.205672	-0.499479	Model>Static Structural>Solution>Contact Tool>Pressure	30-May-19 1:21 PM

Fig. 5.6: Semi minor axis ‘b’ (without wear)

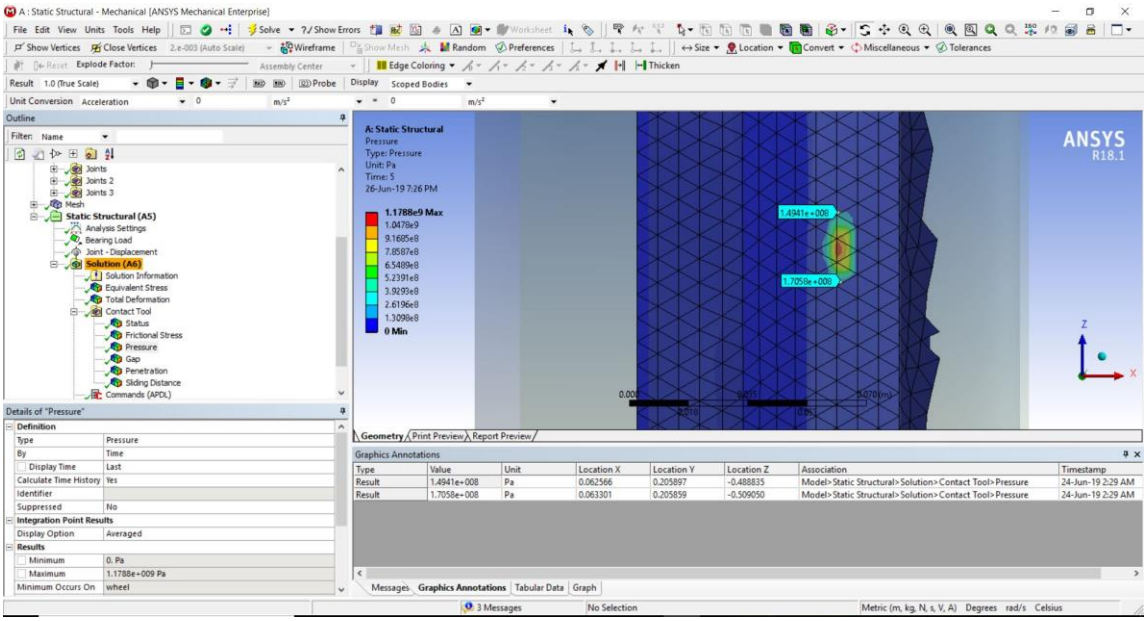

Type	Value	Unit	Location X	Location Y	Location Z	Association	Timestamp
Result	1.4941e+008	Pa	0.062566	0.205897	-0.488835	Model>Static Structural>Solution>Contact Tool>Pressure	24-Jun-19 2:29 AM
Result	1.7058e+008	Pa	0.063301	0.205859	-0.509050	Model>Static Structural>Solution>Contact Tool>Pressure	24-Jun-19 2:29 AM

Fig. 5.7: Semi major axis ‘a’ (wear)

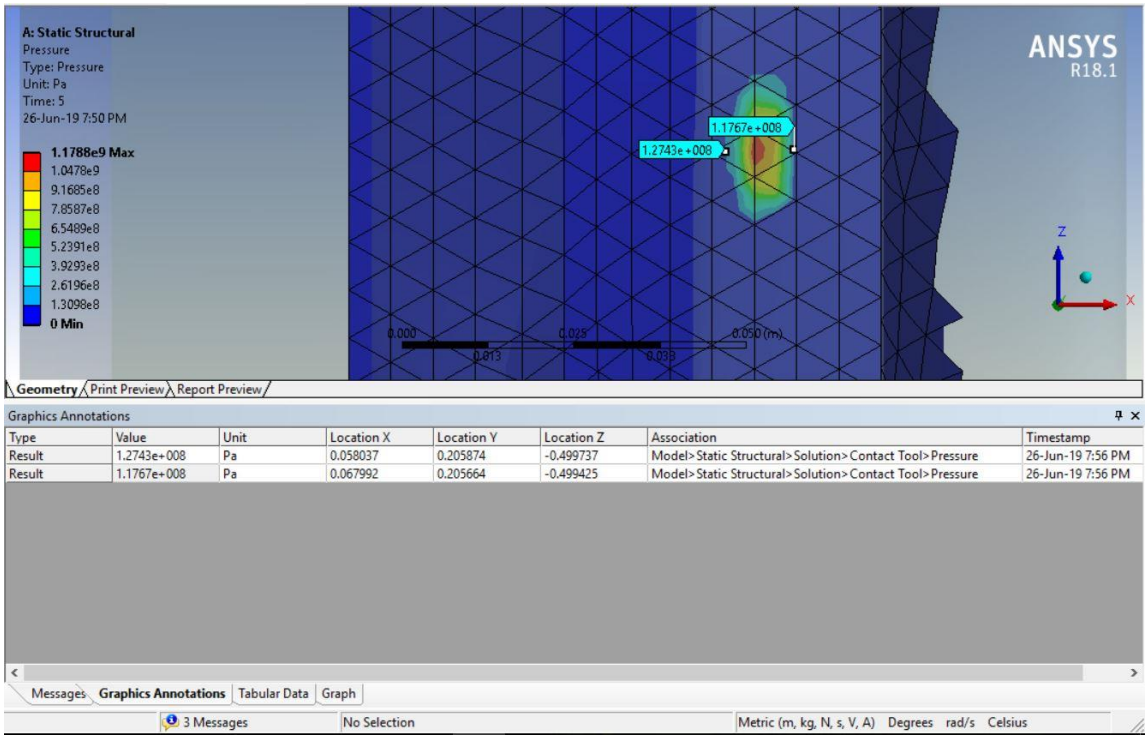

Fig. 5.8: Semi minor axis ‘b’ (wear)

5.2.4. Contact Status

Contact status shows the region with at interface which are far, near, sliding or sticking. As we know that region of contact patch suppers from high pressure intensity, hence sticking occurs at the region which is near to center of contact patch.

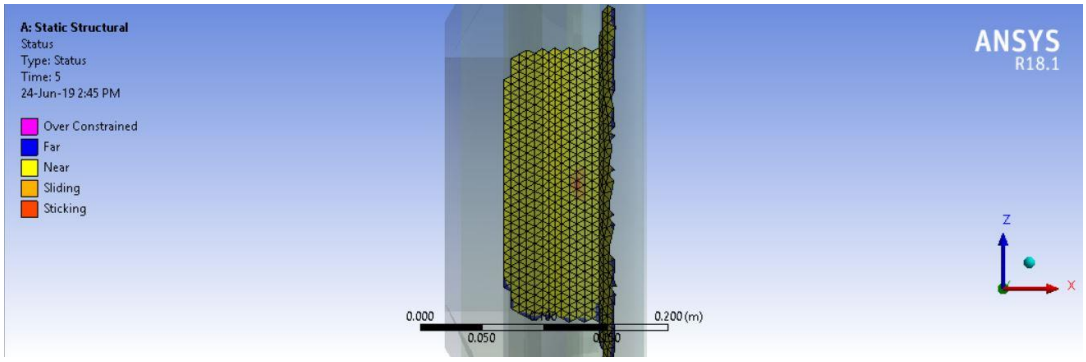

Fig. 5.9: Contact Status between rail and wheel interface

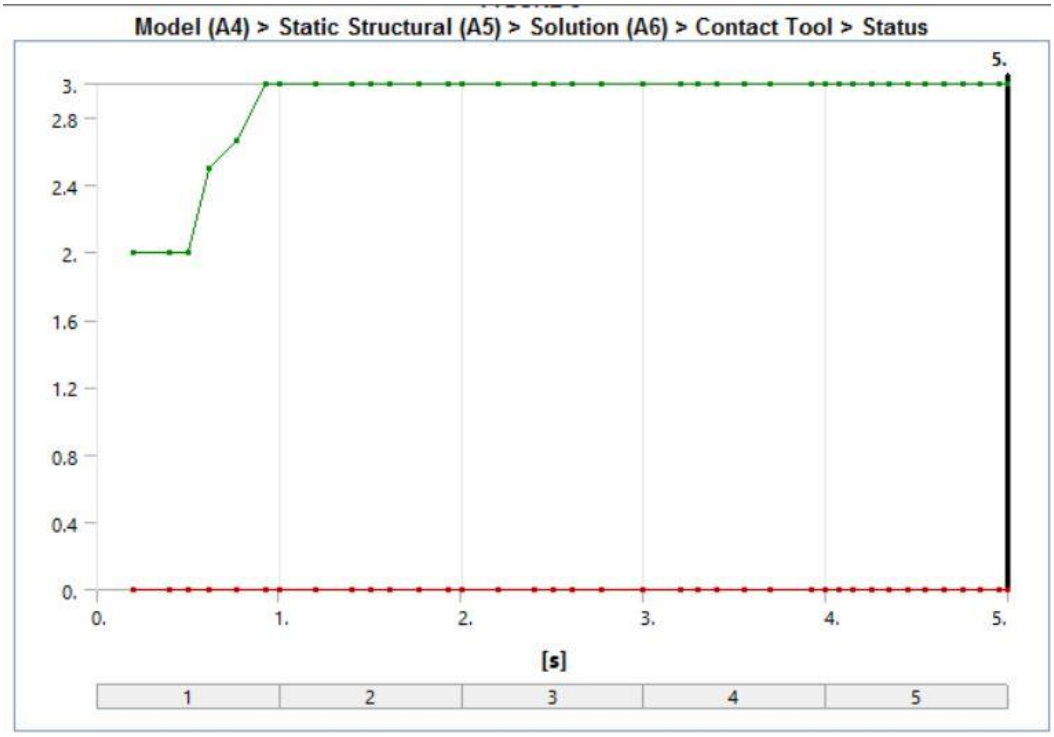

Fig. 5.10: Contact status between rail and wheel

5.2.5. Penetration at contact Region

Penetration phenomenon is high at the regions, where contact patch intensity is high i.e. at the center and surrounding area of contact patch. Although, penetration value is very less i.e. 0.026 mm. This is maximum value of penetration which after reaching a steady state does not see much variation as shown by fig 4.7.

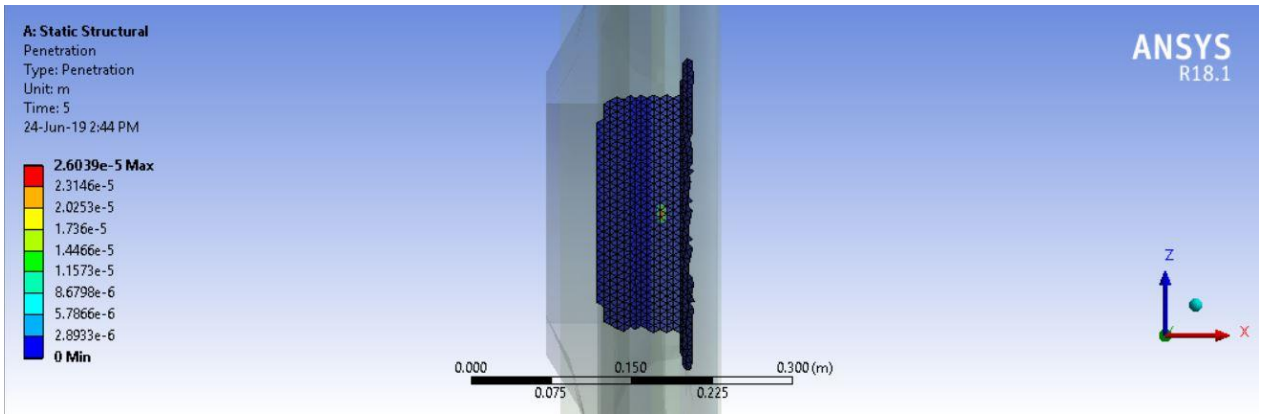

Fig. 5.11: Penetration occurring at rail and the wheel interface

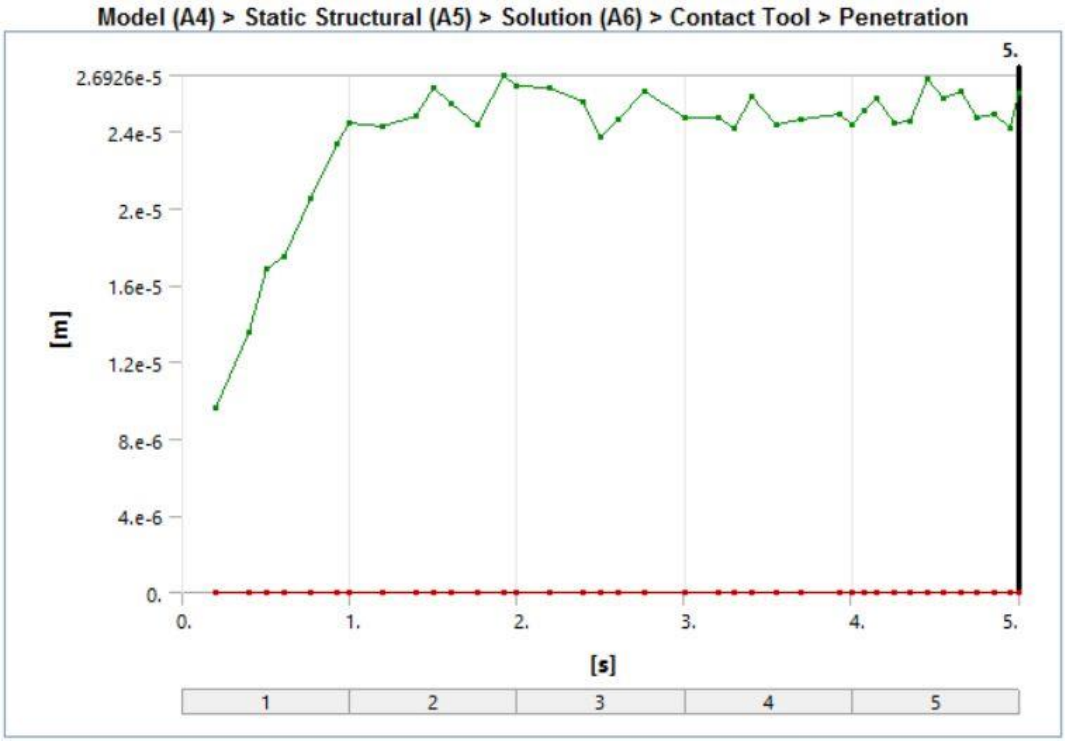

Fig. 5.12: Variation of penetration at contact region w.r.t. to time

5.3 Comparison of analytical and computational results

Table 5.1: Comparison of FEM and Hertz Contact Stress

Maximum Contact Pressure (FEM)	Maximum Contact Pressure (Hertz Contact Model)
1297 MPa (without wear)	1476 MPa
1239 MPa (with wear)	

Table 5.2: Comparison of FEM and Hertz Contact Patch Size

	FEM (wear) (mm)	FEM (without wear) (mm)	Hertz contact theory (mm)
Semi major axis 'a'	10.811	9.948	7.66134
Semi minor axis 'b'	4.977	4.389	4.2198

Percentage error in Maximum contact pressure results = $\left(\frac{1297-1476}{1476}\right)*100$

= -12.12 %

The reason for percentage error in the solution can be attributed to the fact that the geometrical parameters (shape and size) of contact patch defined by Hertz does not changes during the course of the motion between the contacting surfaces, which makes predictions far from reality.

Area of patch (wear) = 169.0376 mm^2

Area of patch (with wear) = 137.0167 mm^2

Area of patch (Hertzian) = 101.5655 mm^2

CHAPTER 6: CONCLUSION

The interacting surfaces are very large in size as compared to the contact patch formed between the interfaces. Therefore the entire load passes through this small contact region. Due to this phenomenon, high stresses are produced between the surfaces as verified by current study and high probability of stress concentration becomes ubiquitous.

FEM approach is followed in this study and compared with analytical formula. By solid modeling all the complicated geometry can be drafted and subsequently imported to FEM solver which provide ample number of control settings (like contact stiffness, contact tolerance, assigning of contact and target bodies, etc.) for maneuvering the contact between interfaces. Hence, FEM enables the user to command complicated geometries in contact.

When wear sub - routine was added to contact definition. A decrease in contact pressure was observed when compared with the simulation which had no wear initialization. This occurs because due to wear contact patch size increases and for the same load. Therefore, contact pressure value decreases.

Most of the contact simulation results reached steady state after 1 second of transient response, this phenomenon is attributed to fact that very fine face meshing was selected, which helps in absorption energy during rebound due to impact loads produced during motion of wheel and hence fine surface meshing helped in not only in more accurate results but also maintenance of healthy contact during the simulation.

Contact parameters of rail – wheel interface has been evaluated and studied. Contact interface geometry plays crucial role in determining magnitude of pressure distribution as shown by Hertzian method. Contact patch size is in form of an ellipse as suggested by the Hertzian theory and pressure distribution shows that contact pressure reaches its maximum value at the center of the elliptical patch which confirms equations suggested by Hertz.

REFERENCES

[1] http://www.indianrailways.gov.in/railwayboard/uploads/directorate/stat_econ/IRSP_2016-17/Annual_Report_Accounts_Eng/Statistical_Summary.pdf

[2] http://www.indianrailways.gov.in/railwayboard/uploads/directorate/stat_econ/IRSP_2016-17/Year_Book_Eng/2.pdf

[3] R.V. Dukkipati, V. Garg, 'Dynamics of railway vehicle systems', New York, NY: Elsevier, 1984.

[4] L. Ramanan, R.K. Krishna, R. Sriraman, 'Thermo-mechanical finite element analysis of a railway wheel', International Journal of Mechanical Sciences, Vol. 41, no. 4-5, pp.487-505, Apr. 1999.

[5] F.D. Fischer, W. Yan, 'Applicability of the Hertz contact theory to rail-wheel contact problems', Archive of applied mechanics, Vol. 70, no. 4 , pp.255-268, May 2000.

[6] T. Telliskivi, U. Olofsson, 'Contact mechanics analysis of measured wheel-rail profiles using the finite element method', Proceedings of the Institution of Mechanical Engineers, Part F: Journal of Rail and Rapid Transit, Vol. 215, no. 2, pp.65-72, Mar. 2001.

[7] B. Xu, H. Sehitoglu, Y. Jiang, 'Three-dimensional elastic-plastic stress analysis of rolling contact', Journal of Tribology, Vol. 124, no. 4, pp.699-708, Oct. 2002.

[8] F.D. Fischer, and M. Wiest, 'Approximate analytical model for Hertzian elliptical wheel/rail or wheel/crossing contact problems', Journal of Tribology, Vol. 130, no. 4: 044501, Oct. 2008.

[9] E. Kassa, H. Ossberger, J.C.O. Nielsen, M. Wiest, W. Daves, 'Assessment of methods for calculating contact pressure in wheel/rail switch contact', Wear, Vol. 265, no. 9-10, pp.1439-1445, Oct. 2008.

[10] L. Wu, W. Li, X. Jin, Z. Wen, 'Thermo-elastic-plastic finite element analysis of wheel/rail sliding contact', Wear, Vol. 271, no. 1-2, pp.437-443, May 2011.

[11] M.A. Arslan, O. Kayabaşı, "3-D Rail–Wheel contact analysis using FEA" Advances in Engineering Software, Vol. 45, no. 1, pp.325-331, Mar. 2012.

[12] M. Dhanasekar, N. Zong, ‘Analysis of rail ends under wheel contact loading’, International Journal of Aerospace and Mechanical Engineering, Vol. 6, pp.452-460, 2012.

[13] M.S. Sichani, ‘Wheel-rail contact modelling in vehicle dynamics simulation’, Doctoral dissertation, KTH Royal Institute of Technology, 2013.

[14] C. Marte, C. Sommitsch, G. Trummer, K. Six, P. Dietmaier, ‘An approximate model to predict near surface ratcheting of rails under high traction coefficient’, Wear, Vol. 314, no. 1-2, pp.28-35, June 2014.

[15] J. P. Srivastava, P. K. Sarkar, and V. Ranjan. ‘Contact stress analysis in wheel–rail by Hertzian method and finite element method’, Journal of The Institution of Engineers (India): Series C, Vol. 95, no. 4, pp.319-325, Oct. 2014.

[16] A. Kumar, S.K. Sharma, ‘A comparative study of Indian Railways and worldwide railways’, International Journal of Mechanical Engineering and robotics Research, Vol. 1, no. 1, pp.114-120, 2014.

[17] C.L. Pun, G. Kang, P. Mutton, Q. Kan, W. Yan, ‘An efficient computational approach to evaluate the ratcheting performance of rail steels under cyclic rolling contact in service’, International Journal of Mechanical Sciences, Vol. 101, pp.214-226, Oct. 2015.

[18] A. Kumar, S.K. Sharma, ‘Dynamics analysis of wheel rail contact using FEA’, Procedia Engineering, Vol. 144, pp.1119-1128, Jan. 2016.

[19] B. Debroy, K. Desai, ’Fund deployment framework for Rashtriya Rail Suraksha Kosh (RRSK)-A Discussion Note’, pp.1-25, 2016.

[20] C. Sommitsch, C. Marte, G. Trummer, K. Six, P. Dietmaier, ‘Modelling surface rolling contact fatigue crack initiation taking severe plastic shear deformation into account’, Wear, Vol. 352, pp.136-145, Apr. 2016.

[21] E.G. Vadillo, J. Blanco-Lorenzo, J. Santamaria, N. Correa., ‘On the influence of conformity on wheel-rail rolling contact mechanics’, Tribology Internationals, Vol. 103, pp.647-667, Nov. 2016.

[22] E.G. Vadillo, J. Blanco-Lorenzo, J. Santamaria, N. Correa, ‘A contact mechanics study of 3D frictional conformal contact’, Tribology Internationals, Vol. 119, pp.143-156, Mar. 2018.

[23] K. Gavril, M. Ciotlaus, M. Vladimir , O. Zsolt, ‘Rail-wheel interaction and its influence on rail and wheels wear’, Procedia Manufacturing, Vol. 32, pp.895-900, Jan. 2019.

[24] A.K. Hunter, H.P. Brunskill, R.S. Dwyer-Joyce and R. Lewis, S. Fukagai, ‘Transitions in rolling-sliding wheel/rail contact condition during running-in’, Tribology International, Mar. 2019.